

Research Article

Towards a Prototype of a Spherical Tippe Top

M. C. Ciocci,¹ B. Malengier,² B. Langerock,³ and B. Grimonprez⁴

¹ Howest, ELIT, University College West Flanders, G. K. De Goedelaan 5, 8500 Kortrijk, Belgium

² Department of Mathematical Analysis, Research Group NaM2, University of Ghent, Galglaan 2, 9000 Ghent, Belgium

³ Department of Architecture, Sint-Lucas Visual Arts, Institute for Higher Education in the Sciences and the Arts, 9000 Ghent, Belgium

⁴ Howest, Industrial Design Center, University College West Flanders, Marksesteenweg 58, 8500 Kortrijk, Belgium

Correspondence should be addressed to M. C. Ciocci, maria-cristina.ciocci@howest.be

Received 14 April 2011; Revised 6 October 2011; Accepted 7 October 2011

Academic Editor: Yuri Sotskov

Copyright © 2012 M. C. Ciocci et al. This is an open access article distributed under the Creative Commons Attribution License, which permits unrestricted use, distribution, and reproduction in any medium, provided the original work is properly cited.

Among spinning objects, the tippe top exhibits one of the most bizarre and counterintuitive behaviours. The commercially available tippe tops basically consist of a section of a sphere with a rod. After spinning on its rounded body, the top flips over and continues spinning on the stem. The commonly used simplified mathematical model for the tippe top is a sphere whose mass distribution is axially but not spherically symmetric, spinning on a flat surface subject to a small friction force that is due to sliding. Three main different dynamical behaviours are distinguished: *tipping*, *nontipping*, *hanging*, that is, the top rises but converges to an intermediate state instead of rising all the way to the vertical state. Subclasses according to the stability of relative equilibria can further be distinguished. Our concern is the degree of confidence in the mathematical model predictions, we applied 3D printing and rapid prototyping to manufacture a “3-in-1 toy” that could catch the three main characteristics defining the three main groups in the classification of spherical tippe tops as mentioned above. We propose three designs. This “toy” is suitable to validate the mathematical model qualitatively and quantitatively.

1. Introduction

Spinning toys are among the most ancient toys, and there is a great variety of them. It is quite simple to start spinning objects like a top or a gyroscope, and though it is simple to explain their motion in general, it is challenging to write down the detailed equations of motion. Among spinning objects, the *tippe top* exhibits one of the most bizarre and counterintuitive behaviours. The commercially available tippe tops, patented in Denmark in the 50s, basically consist of a section of a sphere with a rod. After spinning on its rounded body, the top flips

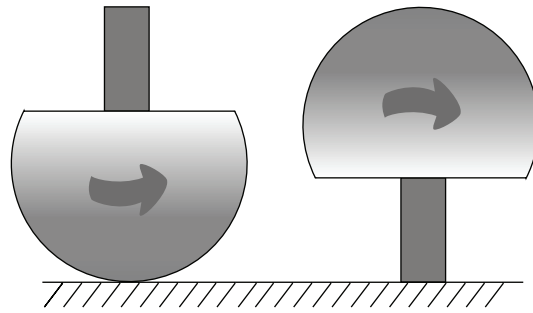


Figure 1: The tippe top, showing inversion.

over and continues spinning on the stem. It is the friction with the bottom surface and the position of the center of mass below the centre of curvature that cause the tippe top to rise its centre of mass while continuing rotating around its symmetry axis (through the stem). See Figure 1 for an illustration. Remarkably, at the inverted state, the center of mass lies higher than at the initial condition, defying gravity. Experimentally, it is known that such a transition occurs only if the initial spin exceeds a certain critical threshold.

The commonly used simplified mathematical model for the tippe top is a sphere whose mass distribution is axially but not spherically symmetric, spinning on a flat surface subject to a small friction force that is due to sliding. Adopting a bifurcation theory point of view we reach a global geometric understanding of the phase diagram of this dynamical system. According to the eccentricity of the sphere and the Jellett invariant (which includes information on the initial angular velocity) six main classes of tops can be identified within three main groups according to the distinguished dynamical behaviours: *tipping*, *nontipping*, and *hanging*; see Figure 3. Note that objects displaying inversion properties such as the tippe top have been known since the 1800s, see, for example, [1]. After the type of tippe top as in Figure 1 was introduced in Denmark, several theoretical articles have been published since then, see, for example, [2–6] for a survey of the literature. Since it was established that sliding friction was necessary to explain the tippe top inversion [2, 7, 8], many studies have been dedicated to the analysis of models for tippe tops, involving linear stability analysis of the relative equilibria, numerical simulations, and so forth. Some studies have addressed the occurrence of transitions between rolling and sliding during the motion, see [3, 4, 9]. In this paper the presented mathematical results mainly reproduce those in [10–15] but our approach is inspired by the hands-on numerical approach as first attempted by Cohen in [2]. We believe this approach is the best choice in giving a clear view of the role of the different parameters that is necessary during the design process of an actual three-dimensional object that effectively demonstrates the model. We remark that in the mathematical model we stick to the common assumption that the only external force acting on the system consists of a normal reaction force and a frictional force of viscous type opposing the motion of the contact point in the supporting plane. This is the most common assumption in the literature, though in [4] the inclusion of a nonlinear Coulomb-type friction is discussed. It is shown there by numerical simulations that the Coulomb term contributes to the tippe top inversion but the effect is weaker compared to the viscous term. The nonlinear Coulomb term results in algebraic destabilization of the initially spinning top, whereas the viscous friction gives exponential destabilization, see also [5]. This argument motivates our choice of including viscous friction only.

The phase diagram and bifurcation diagrams illustrate the main results that confirm the findings described in [10]; the type of asymptotic dynamics is a function of the Jellett invariant (which includes information on the initial angular velocity) and eccentricity of the sphere. Either the asymptotic state is unique or the system is bistable. Three main different regimes are distinguished: no tippe top phenomenon occurs no matter what the initial spin is, tippe top dynamics may occur if the Jellett invariant (which is proportional to the initial spin) is sufficiently large, or *incomplete* tippe top behaviour occurs, where the top rises but converges to an intermediate state instead of rising all the way to the vertical state.

We underline that though the classification results can be obtained in a less cumbersome way by using the Routhian reduction as in [10], the approach used in this paper is standard and straightforward to implement from a prototyping point of view. Also, it is amenable for extensions to include for example transitions from sliding to rolling and vice versa. Our concern in this paper is the degree of confidence in the mathematical model predictions. We wanted to be sure that the mathematical model as presented here and in [10] reflected the reality. Our goal was to investigate if it was possible to make a “3-in-1 toy” that could catch the three main characteristics *tipping*, *nontipping*, and *hanging* that define the three main groups in the classification of spherical tippe tops as mentioned above. As far as we know such a toy does not exist yet. We successfully applied the methodology for efficient use of prototyping during the design process as presented in [16]. To the best of our knowledge this is the first time that 3D printing and rapid prototyping is being applied to design and to produce a “toy” suitable to validate the qualitative and quantitative mathematical model describing the behaviour of a dissipative nonlinear dynamical system. From the bifurcation diagram it was clear that it should be possible to hit three out of the 6 classes of tippe tops (one type for each main group) by keeping one of the characterizing parameters of the system fixed and varying the other. We believe that the realization of an actual toy is a more powerful validation of the model than software simulations which are directly affected by the underlying mathematical idealization assumptions.

Since the two parameters on which the whole classification is based, *inertia ratio* and *eccentricity*, are not independent, the challenge was to come up with a feasible prototype which could be easily mechanically driven. After detailed mathematical calculations and the development of 3D animations (see electronic attachments or <http://cage.ugent.be/~bm/tippetop/tippetop.html>) we used 3D printing to create a functional model giving us a quick and easy hands-on demonstration capability.

2. Mathematical Results

In this paper we consider a sphere whose mass distribution is axially but not spherically symmetric, spinning on a flat surface subject to a small friction force that is due to sliding. In [13], Ebenfeld and Scheck presented a detailed analysis of the dynamics of the eccentric spinning sphere on a flat surface where friction is assumed to be only due to sliding, see also [14]. Without making any other assumptions, we show that their results imply a full qualitative understanding of the asymptotic long-term dynamics. Whereas the treatment of [13, 14] is mainly analytical, here we adopt a bifurcation theory point of view leading to a global geometric understanding of the phase diagram. The phase diagram in Figure 2 and bifurcation diagrams in Figure 3 illustrate our main results. Recall that an ω -limit set of a dynamical system is a closed invariant set that is accumulated by a (forward) trajectory [17]. Our main result is summarized in the following theorem.

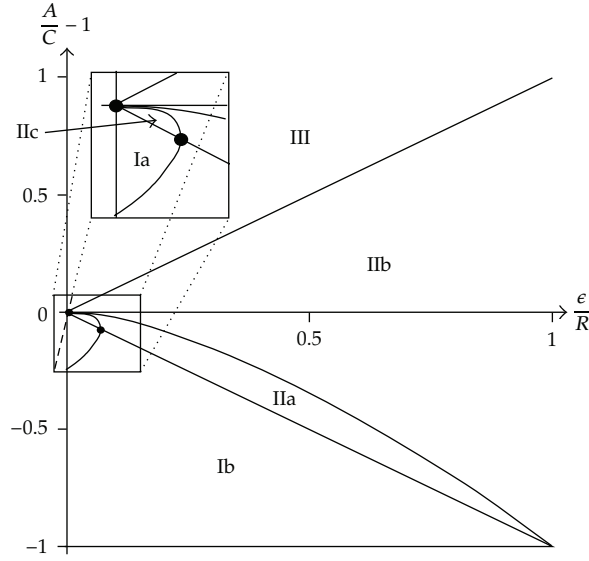


Figure 2: Phase diagram for the dynamics of the eccentric sphere with small sliding friction. The regions of the phase diagram correspond to the qualitative types of bifurcation diagrams of $SO(2) \times SO(2)$ relative equilibria in Figure 3.

Theorem 2.1. *A spinning eccentric sphere on a flat surface with small slipping friction admits three types of (asymptotically stable) ω -limit sets:*

- (i) *vertically spinning top ($\theta = 0$), which has its center of mass straight below its geometric center,*
- (ii) *vertically spinning top ($\theta = \pi$), which has its center of mass straight above its geometric center,*
- (iii) *intermediate spinning top ($0 < \theta < \pi$), whose center of mass is neither straight below nor straight above its geometric center.*

These are solutions of constant energy that are purely rolling due to the assumption on sliding friction (i.e., they display no slipping). The vertical states are periodic, whereas, in general, the intermediate states are quasiperiodic.

At most two of the above types of solutions can be stable at the same time. In case the stable solution is unique its basin of attraction consists of almost the entire phase space (subset of full measure). If the system is bistable, the separatrix between the two different domains of attraction for the asymptotically stable states is expected to be formed by the stable manifold of an unstable intermediate spinning top solution.

All the analytical results needed to arrive at this conclusion can in principle be found in [13, 14]. However, these papers stop short of drawing the full global conclusions as formulated in the above theorem, and also crucially they did not present the phase diagram and bifurcation diagrams that we present in Figures 2 and 3.

We note that for the eccentric sphere in regime I, the state $\theta = 0$ is always asymptotically stable and thus does not display the tippe top phenomenon. Similarly, no such dynamics arises in regime III since there the inverted state $\theta = \pi$ is always unstable. Tippe top

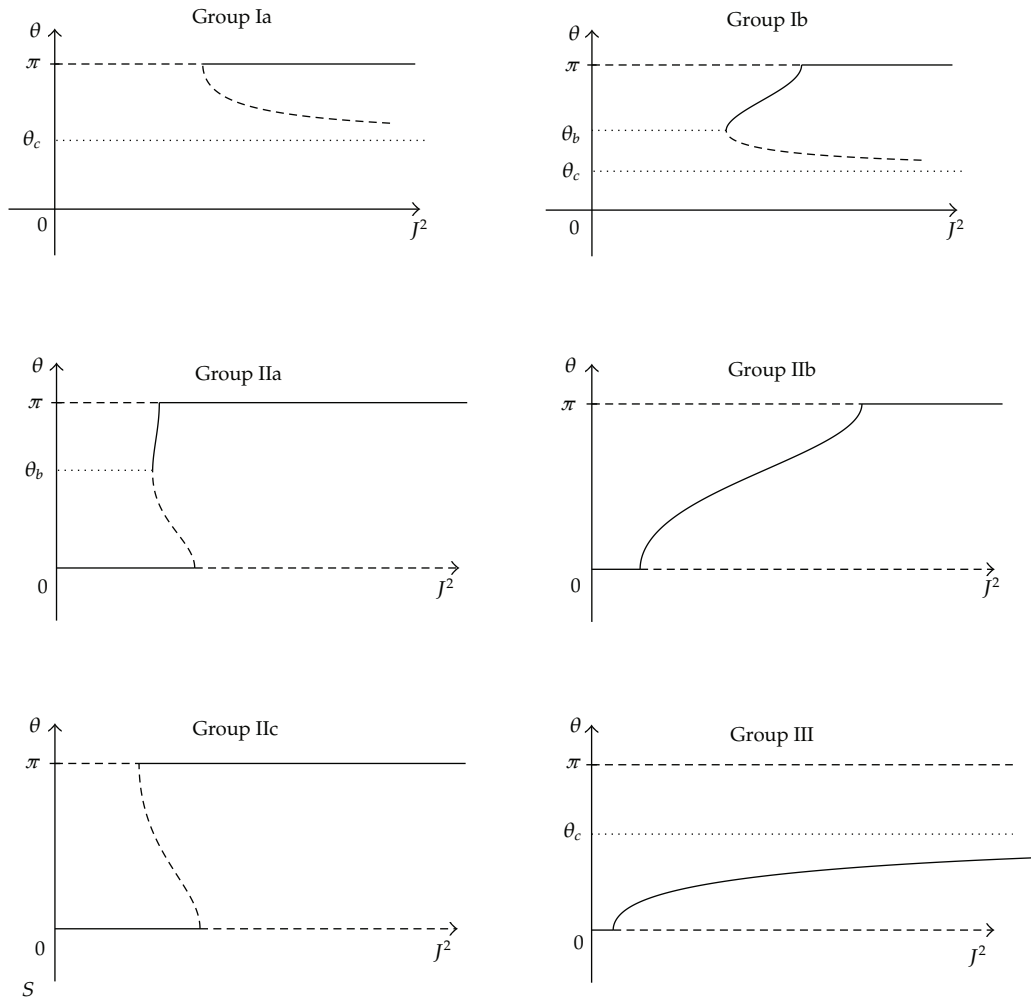


Figure 3: Qualitative bifurcation diagrams of $SO(2) \times SO(2)$ relative equilibria, for the different regions in the phase diagram of Figure 2. Solid black branches correspond to stable relative equilibria, while dashed black branches correspond to unstable ones. The vertical states $\theta = 0$ and $\theta = \pi$ always exist, from which intermediate states (with $0 < \theta < \pi$) may branch off.

dynamics may occur in regime II if the Jellett invariant (which is proportional to the initial spin) is sufficiently large, corresponding to the empirical observation that tippe top dynamics requires a sufficiently large initial spin. In the subregimes IIb and III it is also possible to observe *incomplete* tippe top behaviour, where the top rises but converges to an intermediate state instead of rising all the way to the vertical state $\theta = \pi$. Note that, in regime I, tipping might occur if the top is initially spun sufficiently fast under an angle not close to $\theta = 0$.

It is important to recognize the existence of symmetries. Recall that symmetries are transformations of the phase space that map solutions of a system to other solutions. In our model of the eccentric sphere on a flat surface, symmetries arise due to the homogeneity of the surface on which the sphere moves and the rotational symmetry of the eccentric sphere. The combined symmetries are thus the Euclidean group $E(2)$ (acting as translations and rotations

in the xy plane) and the rotation group $SO(2)$ acting as rotation of the sphere around its axis of symmetry.

It turns out that the ω -limit sets mentioned above are all relative equilibria with respect to the symmetry group $SO(2) \times SO(2) < E(2) \times SO(2)$, see Section 4. Recall that relative equilibria with respect to a group Σ are equilibria for the associated flow on a reduced phase space that is obtained from the original phase space by taking the quotient with respect to the action of Σ . The existence and type of such relative equilibria depend solely on the inertia ratio, the eccentricity of the sphere, and the Jellett integral of motion. We identify a number of regimes characterizing the relative equilibria as a function of the Jellett invariant (which is proportional to the initial angular velocity). The vertical states $\theta = 0$ and $\theta = \pi$ are always $SO(2) \times SO(2)$ relative equilibria and their stability depends on the inertia ratio, the eccentricity of the sphere, and the Jellett integral of motion. In addition, intermediate states may exist, which branch off from the vertically spinning solutions. We sketch the phase diagram in Figure 2. For the labeled regions in this phase diagram, the corresponding bifurcation diagrams for the relative equilibria are presented in Figure 3.

The proof of Theorem 2.1, which builds upon the results by [13, 14], can be found in the appendix. In order to present our point of view clearly and in a self-contained way, in Section 3 we also present a derivation of the equations of motion of the eccentric sphere model of the tippe top, including a discussion of the symmetries and their consequences. Here also, one finds a precise description of the assumed nature of the friction and a definition of all the relevant variables that appear as parameters in Figures 2 and 3. In Sections 4 and 5 the relative equilibria of the system and their stability are discussed. The readers who are acquainted with the topic can start reading from Section 6.

We would like to point out that the strategy of proof used here may well be applicable to a large number of similar examples of mechanical systems under the influence of some kind of friction, such as the *Rattleback* [18] or *Hycaro* tippe top of Tokieda [19]. The key observation is that for mechanical systems under the influence of friction, in a natural way the energy becomes a *Lyapunov function* since friction causes energy loss. The next observation is that orbits which do not dissipate energy need to lie entirely on a subvariety of the phase space that is defined by the condition that friction is absent. Equilibria naturally lie on this subset since they have zero velocity and friction is absent at zero velocity. However, one would expect that typically no solution lies entirely on this subvariety, unless the solution lies on the orbit of a symmetry group that leaves the zero friction subvariety invariant. (One can make this precise by constructing a small local perturbation that moves a solution off the zero friction subvariety.) In many cases, the set of such relative equilibria can be accurately analyzed, either analytically or numerically, and the local stability properties can be deduced from a dissipation-induced instability point of view, based on the local stability properties of the relative equilibria in the absence of friction. We note in this respect that the set of ω -limit sets on the zero friction subvariety is independent of the form and size of the friction. The final step is to draw global conclusions from this local information. The latter is within reach if one has a good understanding of the ω -limit sets. We would like to stress that Theorem 2.1 concerns the asymptotic dynamics. In an experiment with small friction, the observation may well be dominated by *transient* dynamics which bears strong resemblance (on short time scales) to the dynamics of the spherical top without friction. The dynamics of the latter is rather complicated as it is a nonintegrable Hamiltonian system. In Section 7 we present some results from numerical simulations demonstrating explicitly some examples where the transient dynamics does not appear to prevent fast convergence to the asymptotic

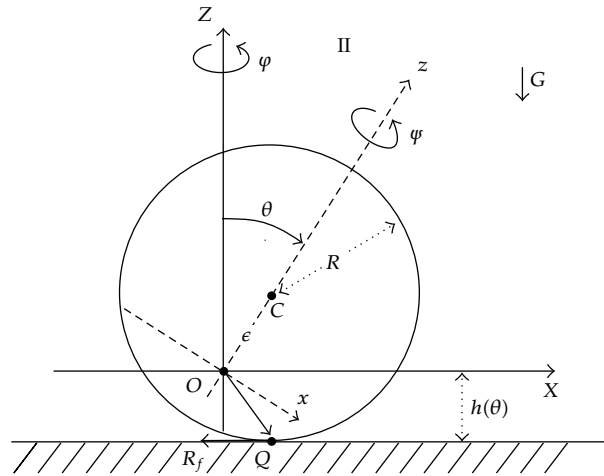


Figure 4: Eccentric sphere version of the tippe top. R is the radius of the sphere, the center of mass O is off center by e . The top spins on a horizontal table with point of contact Q . The axis of symmetry is Oz and the vertical axis is OZ , they define a plane Π (containing OQ) which precesses about OZ with angular velocity $\dot{\varphi}$. The height of O above the table is $h(\theta)$.

states (although of course for sufficiently small friction coefficient the transient dynamics would dominate on finite time intervals).

3. The Equations of Motion

We consider an *eccentric sphere* as in Figure 4, where O denotes the center of mass and C the center of the sphere. The line joining the center of mass and the geometrical center is an axis of inertial symmetry: in the plane perpendicular to this axis the moment of inertia tensor of the sphere has two equal principal moments of inertia.

We describe the motion of the sphere using three reference frames:

- (I) an inertial (laboratory) frame $Mxyz$, where M is some point on the table and the z -axis is the vertical.
- (II) a (noninertial) rotating frame $OXYZ$ whose origin is in the center of mass O and whose 3rd axis is always parallel to the vertical. The X and Y axes are specified below.
- (III) a principal axis system $Oxyz$, whose z -axis is the symmetry axis of the sphere (Note that in [5] the origin of the reference frames (II) and (III) is at the center of the sphere, and not at the center of mass.)

The reference frames (II) and (III) are indicated in Figure 4. The eccentricity e is the distance between the center of mass O and the geometric center C of the sphere, with $0 < e < R$, where R denotes the radius of the sphere. We denote the moments of inertia $I_x = I_y =: A$ and $I_z =: C$. The point of contact with the plane of support is denoted by Q .

Let (θ, φ, ψ) be the Euler angles of the body with respect to OZ , see Figure 5 for an illustration. The OzZ -plane Π contains the vector $\mathbf{q} = OQ$ which joins the center of mass to the point of contact. The plane Π is inclined at angle φ to the vertical Mxz -plane and precesses with angular velocity $\dot{\varphi}$ around the vertical OZ . We choose the horizontal OX in Π so that OY

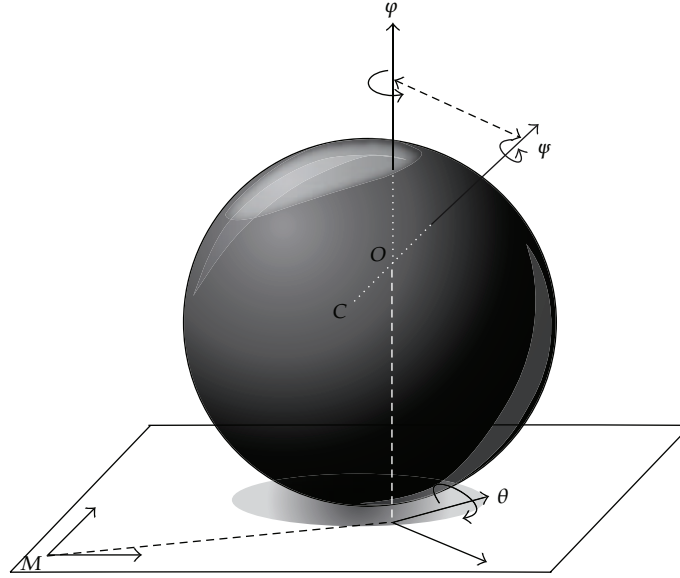


Figure 5: Euler angles (φ, θ, ψ) to fully determine the body, given the coordinates of the center of mass O in an inertial frame with center M .

is perpendicular to Π . For the rotating frame, Ox is in Π and perpendicular to the symmetry axis Oz and the axis Oy coincides with OY . (Note that the axes Ox and Oy are principle axes, but they are not body fixed.) The angle between the vertical OZ and the axis Oz of the top is denoted by θ . The angular velocity $\dot{\theta}$ describes the nutation of the body in the vertical plane Π . The angle φ describes the orientation of the body with respect to the $OXYZ$ frame and $\dot{\varphi}$ is the spin of the sphere around its symmetry axis. We denote by $\mathbf{e}_1, \mathbf{e}_2, \mathbf{e}_3$ the unit vectors along OX, OY , and OZ and by \mathbf{i}, \mathbf{j} , and \mathbf{k} those along Ox, Oy , and Oz . Note that $\mathbf{e}_2 = \mathbf{j}$. Because of the inherent translational symmetry (of the body on the plane), it is convenient to describe the body in terms of the relative (moving) reference frames (II) and (III), rather than in the absolute reference frame (I). By doing so we thus ignore the translational motion on the plane and focus on the relative motion of the body, which captures the tippe top behaviour.

The (relative) position vector of the body is

$$\mathbf{x} = x\mathbf{i} + y\mathbf{j} + z\mathbf{k} = X\mathbf{e}_1 + Y\mathbf{e}_2 + Z\mathbf{e}_3, \quad (3.1)$$

or $\mathbf{x} = (x, y, z)_{Oxyz} = (X, Y, Z)_{OXYZ}$. Note that the coordinates of the reference frames (II) and (III) are related by the relations

$$\begin{aligned} x &= X \cos(\theta) - Z \sin(\theta), \\ y &= Y, \\ z &= X \sin(\theta) + Z \cos(\theta). \end{aligned} \quad (3.2)$$

The reference frames (II) and (III) rotate with respective angular velocities

$$\begin{aligned}\boldsymbol{\Omega}_{II} &= (0, 0, \dot{\psi})_{OXYZ} = (-\dot{\psi} \sin(\theta), 0, \dot{\psi} \cos(\theta))_{Oxyz'} \\ \boldsymbol{\Omega}_{III} &= (-\dot{\psi} \sin(\theta), \dot{\theta}, \dot{\psi} \cos(\theta))_{Oxyz'}.\end{aligned}\quad (3.3)$$

The angular velocity of the body $\boldsymbol{\omega}$ involves, in addition, the angular velocity $\dot{\psi}$:

$$\begin{aligned}\boldsymbol{\omega} &= -\dot{\psi} \sin(\theta) \mathbf{i} + \dot{\theta} \mathbf{j} + n \mathbf{k} \\ &= \dot{\psi} \sin(\theta) \mathbf{e}_1 + \dot{\theta} \mathbf{e}_2 + (\dot{\psi} + \dot{\psi} \cos(\theta)) \mathbf{e}_3 \\ &= (n - \dot{\psi} \cos(\theta)) \sin(\theta) \mathbf{e}_1 + \dot{\theta} \mathbf{e}_2 + (\dot{\psi} \sin^2(\theta) + n \cos(\theta)) \mathbf{e}_3,\end{aligned}\quad (3.4)$$

where $n := \dot{\psi} + \dot{\psi} \cos(\theta)$ denotes the component of $\boldsymbol{\omega}$ about Oz , better known as the *spin*. For later use we introduce the notation $\boldsymbol{\omega} = (\omega_i, \omega_j, \omega_k)$. Consequently, with \mathbf{I} denoting the inertia tensor of the sphere, the angular momentum of the sphere is given by

$$\begin{aligned}\mathbf{L} = \mathbf{I}\boldsymbol{\omega} &= -A\dot{\psi} \sin(\theta) \mathbf{i} + A\dot{\theta} \mathbf{j} + Cn \mathbf{k} \\ &= (Cn - A\dot{\psi} \cos(\theta)) \sin(\theta) \mathbf{e}_1 + A\dot{\theta} \mathbf{e}_2 + (A\dot{\psi} \sin^2(\theta) + Cn \cos(\theta)) \mathbf{e}_3.\end{aligned}\quad (3.5)$$

The point of contact Q has coordinates

$$\begin{aligned}Q &= \left(-h^2(\theta) \frac{d}{d\theta} \left(\frac{\cos(\theta)}{h(\theta)} \right), 0, -h^2(\theta) \frac{d}{d\theta} \left(\frac{\sin(\theta)}{h(\theta)} \right) \right)_{Oxyz} \\ &= (\epsilon \sin \theta, 0, \epsilon \cos \theta - R)_{OXYZ} = (R \sin \theta, 0, \epsilon - R \cos \theta)_{Oxyz}.\end{aligned}\quad (3.6)$$

The velocity of the point of contact Q is

$$\mathbf{V}_Q = \mathbf{v}_O + \boldsymbol{\omega} \times \mathbf{q}, \quad (3.7)$$

where $\mathbf{q} = \mathbf{OQ}$ denotes the vector from the center of mass O to the point of contact Q and \mathbf{v}_O is the velocity of the center of mass. We set $\mathbf{v}_O = U\mathbf{e}_1 + V\mathbf{e}_2 + W\mathbf{e}_3$ and use the fact that $Q = (h'(\theta), 0, -h(\theta))_{OXYZ}$ to obtain

$$\begin{aligned}\boldsymbol{\omega} \times \mathbf{q} &= (-\dot{\theta} h(\theta), \sin(\theta)(\epsilon \dot{\psi} + R\dot{\psi}), -\dot{\theta} h'(\theta))_{OXYZ} \\ &= (-\dot{\theta} h(\theta), \sin(\theta)(\epsilon \dot{\psi} + R(n - \dot{\psi} \cos(\theta))), -\dot{\theta} h'(\theta))_{OXYZ}.\end{aligned}\quad (3.8)$$

Hence, we obtain

$$\mathbf{V}_Q = (U - \dot{\theta} h(\theta), V + \sin(\theta)(\epsilon \dot{\psi} + R(n - \dot{\psi} \cos(\theta))), W - \dot{\theta} h'(\theta))_{OXYZ}. \quad (3.9)$$

The fact that the sphere remains in contact with the table is expressed by the (holonomic) constraint

$$z_O = h(\theta) = R - \epsilon \cos(\theta), \quad (3.10)$$

where $h(\theta)$ denotes the height of the center of mass O above the table, compare Figure 4. From this constraint it follows that the \mathbf{e}_3 component of \mathbf{v}_0 is

$$W := \frac{d}{dt} z_0 = \dot{\theta} h'(\theta) = \epsilon \dot{\theta} \sin(\theta) \quad (3.11)$$

so that the Z -component of \mathbf{V}_Q vanishes, consistent with the constraint.

We note that the physical interpretation of \mathbf{V}_Q concerns the phenomenon of *slipping*. In case $\mathbf{V}_Q \neq \mathbf{0}$ the body slips on the surface. In contrast, a rolling motion of the body is characterized by the fact that $\mathbf{V}_Q = \mathbf{0}$.

The equations of motion will be derived, in Newton's spirit, as a consequence of the action of external forces. We distinguish the following forces acting on the sphere

- (i) The gravitational force: $\mathbf{G} = -mg\mathbf{e}_3$, where m is the total mass of the sphere.
- (ii) A force $\mathbf{F}_Q = \mathbf{R}_n + \mathbf{R}_f$ acting on the point of contact Q , where $\mathbf{R}_n = R_n\mathbf{e}_3$, is the normal reaction force at Q (due to the stiffness of the surface) and \mathbf{R}_f is a friction force. For completeness we mention [20] where a mathematical model for the tippe top is proposed taking elasticity properties of the table and tippe top into account.

Friction is the resistive force acting between bodies that tends to oppose and damp out motion. Friction is usually distinguished as being either static friction (the frictional force opposing placing a body at rest into motion) or kinetic friction (the frictional force tending to slow a body in motion). Importantly, we assume that the friction force is entirely due to the slipping of the sphere on the surface and neglect all other sources of friction. Friction forces can be complicated, and there are various models in circulation. We adopt the assumption of *viscous friction* [9, 15, 21] and assume the friction force to be given by

$$\mathbf{R}_f = -\mu R_n \mathbf{V}_Q, \quad (3.12)$$

where μ is the coefficient of *sliding* friction with the dimension of (velocity)⁻¹. \mathbf{R}_f is proportional to the size of the normal reaction force and vanishes smoothly when $\mathbf{V}_Q \rightarrow \mathbf{0}$. (An alternative model for the friction force is the so-called Coulomb friction $\mathbf{R}_f = -\mu R_n (\mathbf{V}_Q / |\mathbf{V}_Q|)$. This model is not appropriate when $\mathbf{V}_Q \rightarrow \mathbf{0}$ due to the singular nature of this force when $\mathbf{V}_Q = \mathbf{0}$.) Euler's equations of motion for the sphere,

$$\frac{d\mathbf{L}}{dt} + \boldsymbol{\Omega} \times \mathbf{L} = \mathbf{q} \times \mathbf{F}_Q, \quad (3.13)$$

govern the evolution of the angular momentum \mathbf{L} in a noninertial reference frame, rotating with frequency $\boldsymbol{\Omega}$, due to the influence of the external torque $\mathbf{q} \times \mathbf{F}_Q$. The equation of motion for the center of mass O in the rotating frame is

$$m \left(\frac{d\mathbf{v}_O}{dt} + \boldsymbol{\Omega} \times \mathbf{v}_O \right) = -\mathbf{G} + \mathbf{F}_Q. \quad (3.14)$$

In terms of the coordinates in reference frame (III) the equations of motion (3.13) yield

$$\begin{aligned} A\ddot{\varphi} \sin(\theta) &= (Cn - 2A\dot{\varphi} \cos(\theta))\dot{\theta} + z_Q F_Y, \\ A\ddot{\theta} &= -\dot{\varphi} \sin(\theta)(Cn - A\dot{\varphi} \cos(\theta)) + Z_Q F_X - X_Q R_n, \\ C\dot{n} &= x_Q F_Y, \end{aligned} \quad (3.15)$$

where $Q = (x_Q, y_Q, z_Q)_{Oxyz} = (X_Q, Y_Q, Z_Q)_{OXYZ}$ and $\mathbf{F}_Q = (F_X, F_Y, F_Z)_{OXYZ}$. From the equation for the motion of the center of mass (3.14), in terms of reference frame (II), we obtain

$$\begin{aligned} m(\dot{U} - \dot{\varphi}V) &= F_X, \\ m(\dot{V} + \dot{\varphi}U) &= F_Y, \\ m\dot{W} &= R_n - mg. \end{aligned} \quad (3.16)$$

Recalling that $W = \dot{\theta}h'(\theta)$, from the last of the latter equations we may derive an expression for R_n :

$$R_n = mg + m \frac{d}{dt} (\dot{\theta}h'(\theta)) = mg + m\epsilon (\ddot{\theta} \sin(\theta) + \dot{\theta}^2 \cos(\theta)). \quad (3.17)$$

The equations of motion (3.15) and (3.16) can be written as a system of six coupled first-order nonlinear ordinary differential equations in the variables $(u, v, \alpha, \varphi, \beta, \theta, n)$, where $\alpha := \dot{\varphi}$, $\beta := \dot{\theta}$, $u := mU$, and $v := mV$.

Setting $m = 1$ for simplicity, these may be arranged in the standard form $\dot{b} = f(b)$ (when $\sin(\theta) \neq 0$)

$$\begin{aligned} \dot{\alpha} &= \frac{1}{\sin(\theta)} \left[\frac{C}{A} n\beta - 2\alpha \cos(\theta)\beta + z_Q \frac{F_Y}{A} \right], \\ \dot{\beta} &= \frac{1}{A} \left[\alpha \sin(\theta)(A\alpha \cos(\theta) - Cn) - R_n X_Q + Z_Q F_X \right], \\ \dot{\theta} &= \beta, \\ \dot{n} &= \frac{x_Q F_Y}{C}, \\ \dot{u} &= \alpha v + F_X, \\ \dot{v} &= -\alpha u + F_Y, \\ \dot{\varphi} &= \alpha, \\ \dot{\psi} &= n - \alpha \cos(\theta). \end{aligned} \quad (3.18)$$

It should be remembered that R_n , F_X , and F_Y are still functions of the other variables. For instance, from (3.17) and (3.18) one finds

$$R_n = \frac{g + \beta^2 h''(\theta) + h'(\theta)\alpha \sin(\theta)(\alpha \cos(\theta) - Cn/A)}{1 + h'(\theta)/A[-h(\theta)\mu(U - \beta h(\theta)) + h'(\theta)]}. \quad (3.19)$$

Recall that we require that $R_n \geq 0$. If this condition fails, the sphere loses contact with the surface. Expressions for F_X and F_Y follow similarly from (3.12).

It is important to recognize that some of the structure of the equations of motion (3.18) is due to symmetry. We recall that the symmetries are the Euclidean group $E(2)$ (acting as translations, rotations, and reflections in the Mxy plane) and the rotation group $SO(2)$ acting as rotation of the sphere around its axis of symmetry. The effect of the Euclidean symmetry is that the right-hand side of the equations of motion contain no reference to the position of the sphere on the surface. In a similar way, due to the rotational symmetry the equations of motion do not depend explicitly on φ . The system can be viewed as three coupled systems, where the coupling is of *skew product* type: the evolution of α, β, θ , and n does not depend on u, v , and φ , and the evolution of u , and v does not depend on φ . Moreover, note that the position of the center of mass relative to the surface (in Mxy coordinates) could in principle be obtained by integrating the velocities u and v over time. Because of the fact that we take friction into account, Noether's theorem does not apply, so the continuous symmetries we observe need not (and do not) give rise to conserved quantities. However, it was discovered by Jellett [8] by an approximate argument, and later proved by Routh [6], that the system (3.18) has the following conserved quantity:

$$J = -\mathbf{L} \cdot \mathbf{q}. \quad (3.20)$$

Indeed, it follows from (3.13) that $(d\mathbf{L}/dt + \boldsymbol{\Omega} \times \mathbf{L}) \perp \mathbf{q}$, so that

$$\frac{d}{dt}J = -\mathbf{L} \cdot \left(\frac{d}{dt}\mathbf{q} + \boldsymbol{\Omega} \times \mathbf{q} \right) = -\underbrace{(Cn - A\dot{\varphi} \cos(\theta))h'(\theta)^2 \frac{d}{dt} \left(\frac{\sin(\theta)}{h'(\theta)} \right)}_{=0} = 0. \quad (3.21)$$

Note that the Jellett invariant can be written as ([10, 15, 21])

$$J = Cn(R \cos(\theta) - \epsilon) + A\dot{\varphi}R \sin^2(\theta). \quad (3.22)$$

4. ω -Limit Sets Are Relative Equilibria

Our aim is to describe the asymptotic dynamics of the eccentric sphere. Recall that a subset of the phase space is an ω -limit set if this set is accumulated by (forward) orbits. While the friction force destroys the Hamiltonian nature of the dynamics, it greatly simplifies the asymptotic dynamics. This follows from the fact that in the presence of friction the energy, which is conserved in the absence of friction, is almost always decreasing along solutions.

The energy is given by $E = T + V$, where $T = T_{\text{rot}} + T_{\text{tr}}$ is the kinetic energy with its rotational and translational part and $V = mgh(\theta)$ is the potential energy. With our choice of

variables we may write $T_{\text{rot}} = (1/2)(A\omega_1^2 + A\omega_2^2 + C\omega_k^2)$ and $T_{\text{tr}} = (1/2)m(\dot{x}^2 + \dot{y}^2 + \dot{z}^2)$, where $\dot{z} = \epsilon m \sin \theta \dot{\theta}$.

Lemma 4.1 (see [13]). *The energy E is a Lyapunov function (recall that a Lyapunov function is nonincreasing along orbits) for (3.18). In particular,*

$$\frac{d}{dt}E = \mathbf{V}_Q \cdot \mathbf{R}_f \leq 0. \quad (4.1)$$

As \mathbf{R}_f is parallel (and opposite) to \mathbf{V}_Q , $(d/dt)E$ vanishes if and only if \mathbf{V}_Q vanishes. Observe that $E(t)$ decreases monotonically and hence is a suitable Lyapunov function. Moreover, $E(t)$ is analytic and therefore along orbits it is either strictly decreasing or constant. The energy E is constant only if $\mathbf{V}_Q = 0$, that is in the absence of friction. Thus, the ω -limit sets must consist of orbits which do not experience friction. We show that such orbits are necessarily *relative equilibria*.

Proposition 4.2. *Solutions have constant energy only if they are relative equilibria with respect to the action of $SO(2) \times SO(2)$.*

Proof. We already concluded that \mathbf{V}_Q needs to be equal to 0 along any orbit in an ω -limit set. A straightforward calculation shows that $\mathbf{V}_Q = (d/dt)\mathbf{V}_Q = 0$ indeed implies that $\dot{\phi} = \dot{X} = 0$, so that such a solution must be an $SO(2) \times SO(2)$ relative equilibrium. \square

This observation is in fact what one would generically expect to find. If M is a submanifold of the phase space that corresponds to the absence of friction, in general it would be quite unexpected to find a nonequilibrium solution that lies entirely inside M .

5. Stability and Bifurcations of Relative Equilibria

Having determined that the relative equilibria are the only possible asymptotic states in the presence of friction, we derive in this section these solutions of constant energy using the explicit equations of motion (3.15)-(3.16), see also [5, 13, 15]. With $\dot{\phi} = \text{constant}$ and $\mathbf{V}_Q = 0$, $\mathbf{R}_f = 0$, the equations of motion yield $\dot{\alpha} = 0$, $\dot{\beta} = 0$, $\beta = 0$, $\dot{n} = 0$, $U = 0$, $W = 0$ and

$$\begin{aligned} \alpha V &= 0, \\ \alpha \sin(\theta)(A\alpha \cos(\theta) - Cn) - mge \sin(\theta) &= 0, \\ V + [R(n - \alpha \cos(\theta)) + e\alpha] \sin(\theta) &= 0. \end{aligned} \quad (5.1)$$

These equations have the following three types of solutions. The linear stability analysis differs from [13, 14] in methodology.

Vertical States

(1) Vertical state $\theta = 0$:

$$\begin{aligned} U = V = 0, \quad \theta = 0, \quad n = \text{arbitrary constant}, \\ \alpha = \dot{\phi} = \text{undefined constant}. \end{aligned} \quad (5.2)$$

The top is spinning about its axle with center of mass straight below the geometric center.

(2) Vertical state $\theta = \pi$:

$$\begin{aligned} U = V = 0, \quad \theta = 0, \quad n = \text{arbitrary constant}, \\ \alpha = \dot{\psi} = \text{arbitrary constant}. \end{aligned} \quad (5.3)$$

The top is spinning about its axle with center of mass straight above the geometric center.

Intermediate States

For these solutions we have $U = V = 0$, $0 < \theta < \pi$, and n , α , and θ are related by

$$n = \alpha \cos(\theta) - \frac{\epsilon}{R} \alpha, \quad (5.4)$$

$$\alpha(A\alpha \cos(\theta) - Cn) - mg\epsilon = 0. \quad (5.5)$$

Elimination of n from the above yields

$$\alpha^2 = \frac{mg\epsilon}{(A - C) \cos(\theta) + C(\epsilon/R)}. \quad (5.6)$$

Hence, the condition for the existence of intermediate states is

$$\left(\frac{A}{C} - 1\right) \cos(\theta) + \frac{\epsilon}{R} > 0. \quad (5.7)$$

It is natural to divide the solutions into three groups, according to regimes of the parameters A/C and ϵ/R [21].

Group I: $A/C < 1 - \epsilon/R$. Intermediate states exist with

$$\theta > \theta_{c_1} = \cos^{-1}\left(\frac{\epsilon/R}{1 - A/C}\right), \quad \text{with } 0 < \theta_{c_1} < \frac{\pi}{2}. \quad (5.8)$$

Group II: $1 - \epsilon/R < A/C < 1 + \epsilon/R$. Intermediate states exist with any $0 < \theta < \pi$.

Group III: $A/C > 1 + \epsilon/R$. Intermediate states exist with

$$\theta < \theta_{c_2} = \cos^{-1}\left(\frac{\epsilon/R}{1 - A/C}\right), \quad \text{with } \frac{\pi}{2} < \theta_{c_2} < \pi. \quad (5.9)$$

As in [10] we further refine this classification. Note that the intermediate states discussed here correspond to the tumbling solutions discussed in [13].

The intermediate states are completely determined by (5.4), (5.5), and the Jellett invariant J . More precisely, combining the square of (3.22) with (5.4) and (5.6), they are obtained by solving

$$f(J^2, \cos \theta) := \frac{J^2}{mg\epsilon CR^2} \left[\left(\frac{A}{C} - 1 \right) \cos(\theta) + \frac{\epsilon}{R} \right] - \left[\left(\cos(\theta) - \frac{\epsilon}{R} \right)^2 + \frac{A}{C} (1 - \cos^2(\theta)) \right]^2 = 0. \tag{5.10}$$

The next theorem summarizes the linear stability and local bifurcation results, as depicted in Figure 3 (cf. [21]), and the proof is sketched in the Appendix. We identify six different groups according to how the value of A/C is related to the eccentricity ϵ/R . In the literature, results have previously been expressed in terms of variables n_0 and n_π , referring to the spin of an initial condition in a vertical state. We define $n_0 := J/C(R - \epsilon)$, which is the value of the spin n at $\theta = 0$ for motion with Jellett invariant J . Similarly, $n_\pi := -J/C(R + \epsilon)$ denotes the spin of the solution with Jellett invariant J at $\theta = \pi$. Note that, for a fixed value of the Jellett invariant J , these spins are related by $n_0 = -n_\pi(R + \epsilon)/(R - \epsilon)$. We further define

$$n_\pm := \sqrt{\frac{\pm m g \epsilon}{C[(1 \pm \epsilon/R) - A/C]}} (1 \pm \epsilon/R), \quad b := \frac{\epsilon/R - \sqrt{(1/3)A/C(1 - A/C - (\epsilon/R)^2)}}{1 - A/C}, \tag{5.11}$$

and $\theta_b := \arccos(b)$. Furthermore we define $c = \epsilon/R/1 - (A/C)$ and $\theta_c := \arccos(c)$.

Theorem 5.1. *The bifurcation diagrams of the eccentric sphere spinning on a flat surface with small friction fall in one of the following six categories (Figure 3).*

Group I: $A/C - 1 < -\epsilon/R$.

- (i) *The vertical state $\theta = 0$ is stable for any value of J .*
- (ii) *The vertical state $\theta = \pi$ is stable if $|n_\pi| > n_+$ and unstable otherwise.*
- (iii) *Intermediate states exist for all values of θ satisfying $\theta > \theta_c$.*

Group Ia: $b < -1$. The entire branch of intermediate states is unstable.

Group Ib: $b > -1$. The branch of intermediate states has a fold point at $\theta = \theta_b$. The branch with $\theta > \theta_b$ is stable, while the branch with $\theta < \theta_b$ is unstable.

Group II: $-\epsilon/R < (A/C - 1) < \epsilon/R$.

- (i) *The vertical state $\theta = 0$ is stable if $|n_0| < n_-$ and unstable otherwise.*
- (ii) *The vertical state $\theta = \pi$ is stable if $|n_\pi| > n_+$ and unstable otherwise.*
- (iii) *Intermediate states exist for all θ . We distinguish the following three subgroups.*

Group IIa: $(A/C - 1) < -(\epsilon/R)^2$ and $|b| < 1$. A fold bifurcation of intermediate states occurs.

Group IIb: $(A/C - 1) > -(\epsilon/R)^2$ or $b > 1$. The entire branch of intermediate states is stable.

Group IIc: $(A/C - 1) < -(\epsilon/R)^2$ and $b < -1$. The entire branch of intermediate states is unstable.

Group III: $(A/C - 1) > \epsilon/R$.

- (i) *The vertical state $\theta = 0$ is stable if $|n_0| < n_-$.*
- (ii) *The vertical state $\theta = \pi$ is unstable for all J .*
- (iii) *Intermediate states exist for $\theta < \theta_c$ and are all stable.*

The proof of Theorem 5.1 can be mainly recovered from [10]; for completeness we provide the calculations based on a direct approach in the appendix.

6. Prototype of a Spherical Tippe Top

Rapid prototyping (RP) technologies enable solid models to be obtained from designs generated with CAD applications. Their increasing popularity in industry is due to the reduction in cost and time associated with the use of these models when verifying product development stages and improvements in end quality. These technologies can also be applied to verify the correctness and/or accuracy of mathematical models and last but not least to enhance students' active learning in the frame of a learning-by-doing approach. Students can bring their designs to fruition and develop a deeper insight in abstract concepts. We made a prototype of a spherical tippe top for educational use in the Product Development Laboratory of Howest.

As pointed out earlier, to realize a 3-in-1 toy an axially symmetric sphere where one has control over A/C and ϵ/R is needed. We considered three possible designs:

- (1) a solid sphere with a cylindrical hole through the center where a setscrew can move;
- (2) a hollow sphere with a cylindrical rod on which a weight can move;
- (3) a hollow sphere with a toroidal band at the equator fitted with a cylindrical rod on which a weight can be screwed.

From the bifurcation diagram in Figure 2, it is clear that it is possible to hit the three main groups by fixing ϵ/R and changing A/C . Therefore, it is important to understand for the three designs how A/C and ϵ vary with respect to each other when the weight is moved. We set up a Maple worksheet based on the given mathematical description and calculated A/C and ϵ in function of the position of the midpoint of the moving weight with respect to the center of the sphere; this will be further on denoted by Z_2 . We took into account the physical parameters: dimensions of the different parts (radii, heights, and thickness) and the density of the materials.

From this we realized that for the solid sphere the goal of the three types is within reach, whereas for the hollow sphere the design has to be modified. Our modifications resulted in the third design as given above. We now discuss our findings for the realized prototypes. Our realizations were all printed with the commercial available Dimension SST1200es with printing technology based on the FDM principle (fused deposition modeling) in ABSplus.

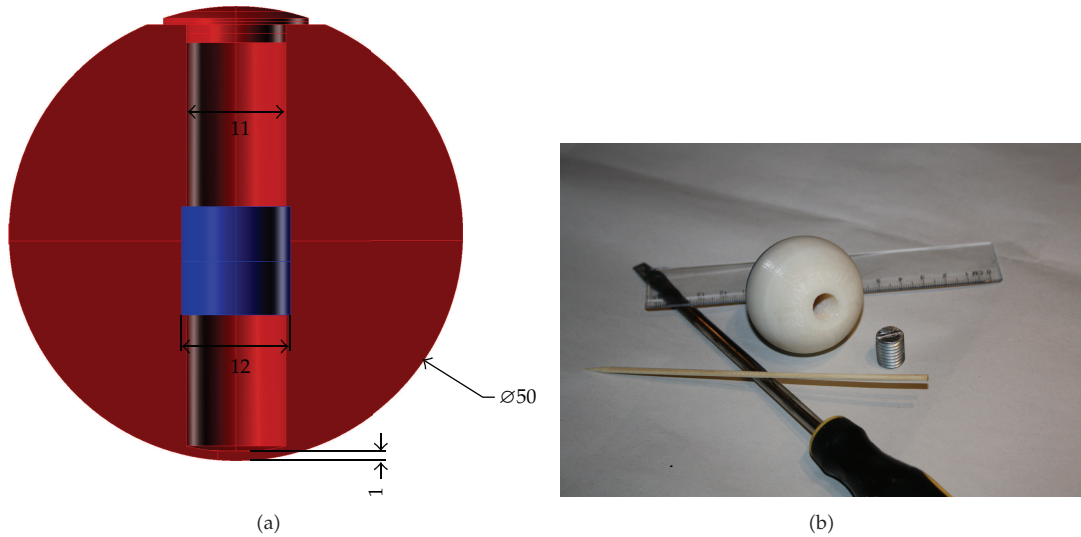


Figure 6: First prototype of a spherical tippe top.

6.1. Sphere with Cylindrical Hole and Setscrew

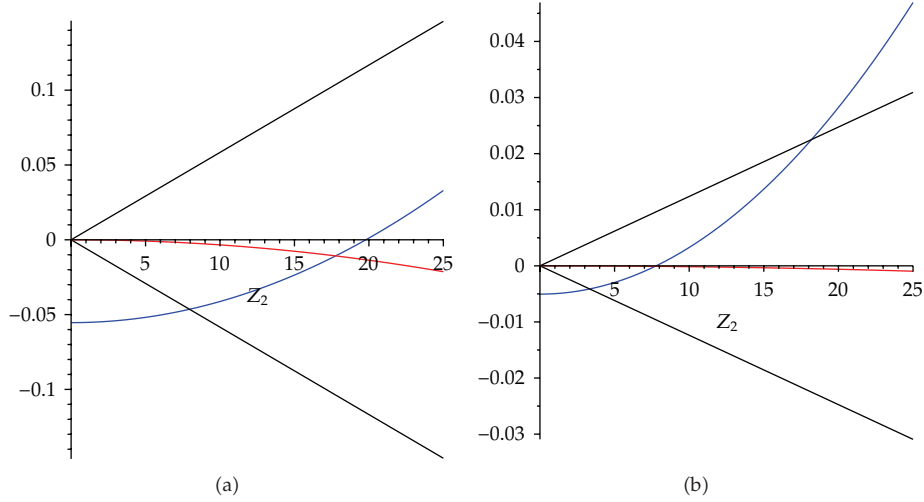
For the first design we realized three different tops, varying the geometrical dimensions. This was done because the calculation showed that for the given materials some zones are hard to achieve or are very narrow, see Figure 7. The prototype consists of a sphere with a cylindrical hole through the center, together with a piece of adjustable cylindrical iron wire (setscrew), see Figure 6. With a caliper, it can be checked how deep the setscrew is set in the hole. The position of the midpoint of the setscrew with respect to the center of the sphere is denoted by Z_2 . The hole is suitable for a setscrew M12. The dimensions of the toy were chosen based on the mathematical calculations derived from the model. The diameter of the sphere was chosen so that one can comfortably spin the toy by hand. With a sphere of diameter 50 mm, good values for the chosen design are a hole of radius 5.5 mm, filled with the setscrew of height 15 mm, or a hole of radius 1.5 mm, filled with the setscrew of height 3 mm, see Figure 7. The densities are 1.08 g/cm^3 for ABSplus and 7.87 g/cm^3 for the setscrew.

The prototype is axially symmetric; therefore, only the eccentricity ϵ and the moment of inertia A are functions of Z_2 , they are easily calculated; C remains constant when moving the setscrew up and down. In Figure 7 the quantities $(A/C) - 1$, $\pm\epsilon/R$, and $-(\epsilon(Z_2)/R)^2$ are plotted as functions of Z_2 , (a) for the prototype with a M12 setscrew and (b) for the prototype with a M3 setscrew. The printed prototype in Figure 6, is of the first type and according to the mathematical calculations will exhibit the predicted behaviour as follows: for Z_2 between 0 mm and 7.95 mm the toy does not show tippe top dynamic no matter what the initial spin is (type I), for Z_2 between 7.95 mm and 17.76 mm complete tippe top dynamic is observed (type IIc). For Z_2 above 17.76 mm the top is of type IIb (incomplete tipping is observed if initial spin is not sufficiently high).

For the different positions of the weight, we launched by hand the toy plenty (≥ 50) of times and registered each time tipping, nontipping, or hanging. In Table 1 we report the typical results for 5 launches. Note that the tippe top is hand spun, so there will be a deviation from the starting position $\theta = 0$. Tipping and nontipping were mostly observed in the setup

Table 1: Hand launched tippe top. Observed occurrences of the different types on 5 launches.

Depth setscrew	17.5	12.5	7.5	2.5	-2.5
Z_2	0	5	10	15	20
Nontipping	5	3	0	0	0
Tipping	0	1	5	4	0
Hanging	0	1	0	1	5
Theory	I (sphere)	I	IIa	IIa	IIb

**Figure 7:** Different tippe top regimes in function of the position Z_2 of the midpoint of the setscrew. The black lines are $\pm\epsilon(Z_2)/R$, the blue curve is $A(Z_2)/C - 1$, and the red curve is $-(\epsilon(Z_2)/R)^2$. On the left, the result for the printed prototype with a M12 setscrew, see Figure 6. On the right, the result for a prototype of the same shape but a setscrew M3.

of type IIa and I, respectively. For the setup of type IIb, the expected behaviour (tipping) was not observed; we always observed the hanging behaviour. This is because we were not able to launch the toy fast enough by hand and also because the setscrew sticking out the toy does not allow ideal launching position. Our observations indicate that the prototype behaves as predicted by the model. In details, tipping and hanging at $Z_2 = 5$ can be explained by the presence of a branch of intermediate states and stable π position that one could hit if the toy is not launched exactly from the $\theta = 0$ position, see Figure 3. The hanging at $Z_2 = 15$ is due to the fact that we did not launch the top fast enough.

For a prototype fit for a M3 screw, the intervals for Z_2 are as follows: for Z_2 between 0 mm and 3.33 mm the toy does not show tippe top dynamic no matter what the initial spin is (type I); for Z_2 between 3.33 mm and 18.20 mm complete tippe top dynamic is observed (type II). For Z_2 above 18.20 mm the top is of type III (incomplete tipping is observed). Also, this prototype was spun ≥ 50 times, and we registered similar observations as for the previous one.

We conclude that this prototype can give a working 3-into-1 toy but has some disadvantages.

- (i) The setscrew can come loose after intensive use.
- (ii) When there are three zones present, at least one of the zones is small.

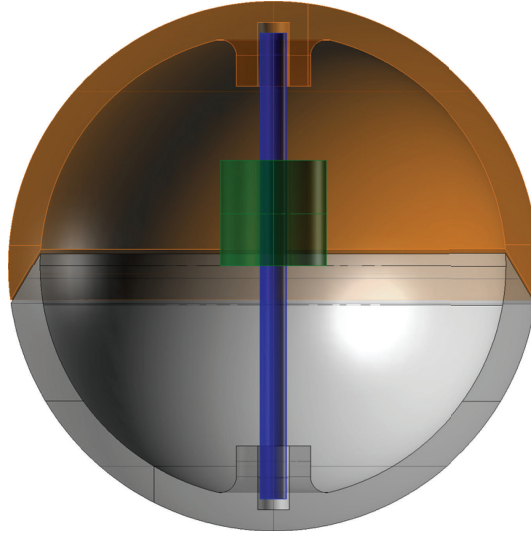


Figure 8: Design of the second prototype.

(iii) Using a caliper to know if the setscrew is in the center is not practical.

Several attempts were done in the computations to improve the design, for example, by adding holes into the solid sphere. These attempts were not successful, so no other prototype was printed. Instead, we concentrated on the sphere with a cylindrical rod.

6.2. Sphere with Cylindrical Rod

The second design consists of a spherical shell with a cylindrical solid rod through the center along which a symmetric bead is spun; this bead can be put at different heights along the rod. In this design, the user must open the sphere and change the position of the weight by screwing it up or down, after which the sphere can be closed and spun. See Figure 8.

The advantage of this design is that different ABS colors can easily be used for both sides making the tipping more visible and that the rod can be marked at the critical positions. Where in the first design setscrews of different length can be used, in this design weights of different lengths and different widths can be considered within one toy. Also, different materials for the rod can be considered.

However, computations show that a 3-into-1 toy was difficult to obtain with the chosen materials: ABS, iron, and nylon. We briefly summarize our findings that form the basis of further improvements that lead to the third prototype. We tried three different possibilities for the rod: iron, nylon, and ABS. Nylon and ABS seem to work best. With an iron rod and physical parameters that allow easy playing with the toy we did not succeed in catching all the three zones. See below for the specific values of the parameters. As Figure 9(a) shows, only zone three is hit, which means that this tippe top never shows complete inversion but may tip up to a certain angle.

The prototype is axially symmetric; therefore, only the eccentricity e and the moment of inertia A are functions of Z_2 , they are easily calculated; C remains constant when moving the weight up and down. The physical parameters for the construction are radius of the

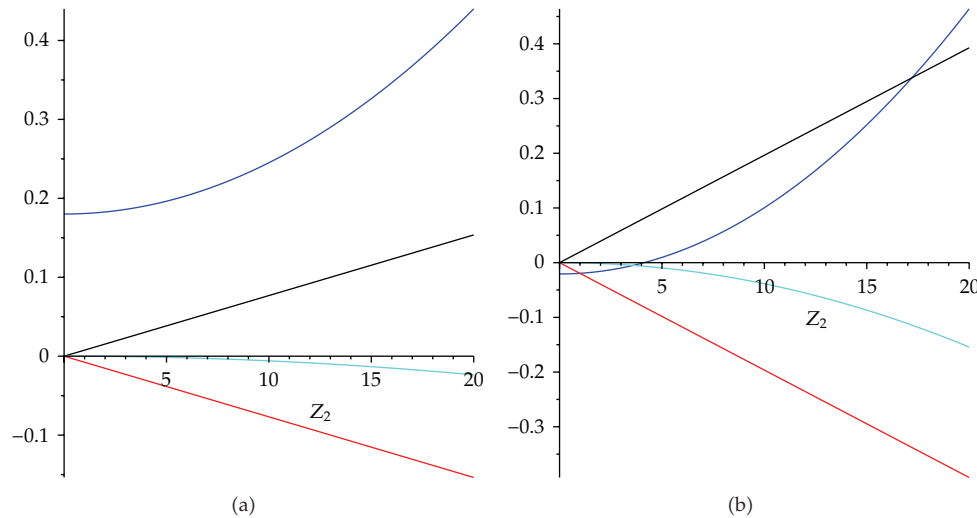


Figure 9: (a) Different tipping top regimes in function of the position of the midpoint of the setscrew. The black lines are $\pm\epsilon(Z_2)/R$, the blue curve is $A(Z_2)/C - 1$, and the red curve is $-(\epsilon(Z_2)/R)^2$. The physical parameters for the construction are radius of the spherical shell in ABS of 25 mm, thickness of the shell of 2.5 mm, radius of the iron cylindrical rod of 3 mm, radius of the (iron) weight of 10 mm, and height of the weight of 10 mm. (b) Different tipping top regimes in function of the position of the midpoint of the setscrew. The black lines are $\pm\epsilon(Z_2)/R$, the blue curve is $A(Z_2)/C - 1$, and the red curve is $-(\epsilon(Z_2)/R)^2$. The physical parameters for the construction are radius of the ABS spherical shell of 25 mm, thickness of the shell of 2.5 mm, radius of the nylon cylindrical rod of 2.5 mm, radius of the (iron) weight of 10 mm, and height of the weight of 10 mm.

spherical shell of 25 mm, thickness of the shell of 2.5 mm, radius of the cylindrical rod of 3 mm, radius of the weight of 10 mm, and height of the weight of 10 mm.

In the case of a nylon or ABS rod, it was possible to obtain a tipping top. As illustrated in Figure 9(b), both zones II and III are hit, which means that complete tipping and incomplete tipping may be observed according to the position of the weight. Note that the section of the blue curve in zone III is very small, which makes it very difficult to observe the hanging phenomenon. A similar observation holds for the section of the blue curve in zone I; this is so small that nontipping behaviour cannot in practice be observed. Many launches of this prototype only confirmed the observations above. This seems to be a good type II tipping top, but we were not able to observe the other behaviours.

6.3. Sphere with a Toroidal Band and a Cylindrical Rod

The third design consists of a spherical shell with a toroidal band around the equator and a cylindrical solid rod through the center along which a symmetric bead is spun. Also in this design, the user must open the sphere and change the position of the weight by screwing it up or down, after which the sphere can be closed and spun. See Figure 10.

Adding a toroidal band was a way to find a compromise between a spherical shell and a solid sphere. The prototype is still axially symmetric, and the band provides a better click system to open and close the toy. The physical parameters for the construction are radius of the spherical shell of 25 mm, thickness of the shell of 3 mm, radius of the cylindrical rod of 3 mm, radius of the weight of 6 mm, and height of the weight of 10 mm. The band has the

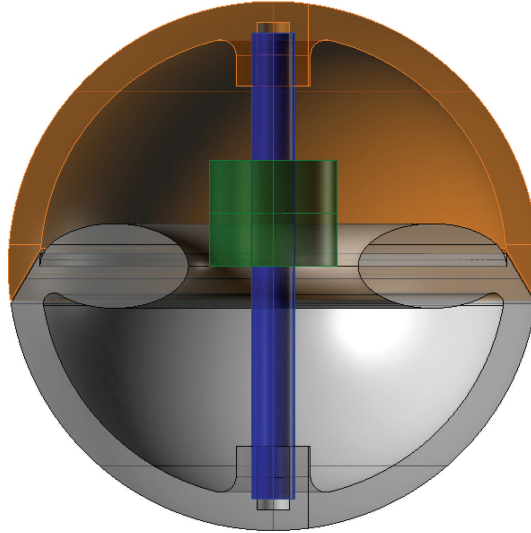


Figure 10: Design of the third prototype.

form of a solid of revolution generated by an ellipse rotating around the rod, the semiaxes of the ellipse measure, respectively, 7 mm and 4 mm. The rod is made of iron. According to the mathematical model, the top should behave as follows: for Z_2 between 0 mm and 4.14 mm the toy does not show tippe top dynamic (type I); for Z_2 between 4.14 mm and 16.8 mm complete tippe top dynamic is observed (type II). For Z_2 above 16.8 mm the top is of type III (incomplete tipping is observed).

The toy was launched many times, allowing to observe without problems zones I and II predicted by the model. Zone III is, however, difficult to observe at first, the maximum Z_2 that can be obtained with the constructed prototype was only 15 mm (due to the fastening system of the rod), and moreover $\theta_c > 2\pi/3$ which is not so easy to see. Different weights can, however, be used so that zone III becomes visible; for example, this is the case when using an iron weight with radius 8 mm and height 5 mm. We conclude that this last prototype is a good candidate for the 3-in-1 toy, although some further optimizations of the physical parameters can be considered (Figure 11).

7. Numerical Illustrations

7.1. System Trajectories

In this section we present some simulations of (3.15)-(3.16). We focus on the parameter regime of Group II since these are the tops exhibiting “tipping” behaviour. Indeed, if the initial spin $|n_0| > \max(n_-, n_2 := n_+(R + \epsilon)/(R - \epsilon))$, then tipping occurs. The trajectories lie in the (reduced) 6-dimensional phase space (we ignore the $\dot{\psi}$ equation); here we show their projections in the 3-dimensional subspace of the variables (α, θ, n) .

Figure 12 shows a number of trajectories for a tippe top of Group IIb starting from initial conditions $u = 0$, $v = 0$, $\theta = 0.01$, $n = \text{arbitrary}$ and $\alpha = (1/2A)(Cn + \sqrt{C^2n^2 + 4Amg\epsilon})$. Other input parameters are $m = g = 1$, the friction coefficient $\mu = 0.04$, the eccentricity $\epsilon/R = 0.3$, and inertia ratio $A/C = 0.92$. Points with $n < n_-$ are stable whereas

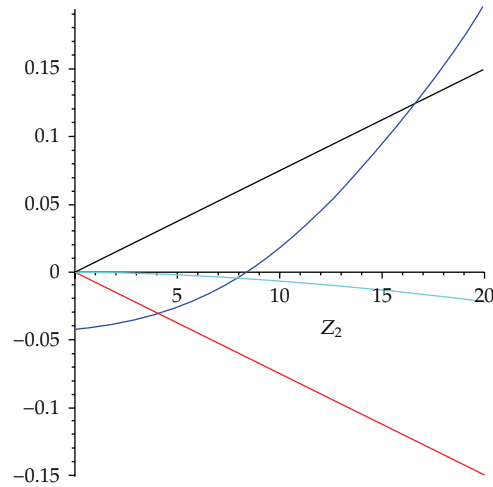


Figure 11: Different tippe top regimes in function of the position of the midpoint of the setscrew. The black lines are $\pm\epsilon(Z_2)/R$, and the blue curve is $A(Z_2)/C - 1$, the red curve is $-(\epsilon(Z_2)/R)^2$. The physical parameters for the construction are here: radius of the ABS spherical shell 25 mm, thickness of the shell 3 mm, radius of the cylindrical rod 3 mm, radius of the (iron) weight 6 mm, height of the weight 10 mm, semi-axis of the ellipse generating the torus 7 mm and 4 mm.

those for which $n > n_-$ are unstable. Let $n_* = -n_+(R + \epsilon)/(R - \epsilon)$ be the value of the initial spin calculated for the angle $\theta = 0$ at the Jellett where the change in stability for the inverted position ($\theta = \pi$) occurs. Trajectories originating near an unstable noninverted position are attracted either to one of the intermediate states at an angle $\theta > 0$ when $n_- < n < n_*$ or when $n > n_*$ to a steady state for which $\theta = \pi$; in this case, the ball rises fully to a stable inverted vertical (tippe top) position with a final spin n determined by the Jellett. The blowups in the insets show oscillations in the immediate neighborhood of the fixed points; these depend on the precise initial conditions. We note also that changing μ does not affect the final destination of the trajectories but it does affect the time needed to follow such trajectories in phase space, this at least within our parameter range of computations.

Figure 14 shows a number of trajectories for a tippe top of Group IIa with friction coefficient $\mu = 0.04$, starting now under an angle close to the inverted position $\theta = \pi$. Physical parameters are $m = g = 1$, $\epsilon/R = 0.5$, and $A/C = 0.55$.

Recall from Figure 3 that trajectories starting near the inverted position will, depending on the initial spin, remain in the neighborhood of $\theta = \pi$ go all the way down to the noninverted position $\theta = 0$, or reach a stable intermediate state. For a clearer overview of the possible behaviours we use the symmetry $(n, \alpha) \rightarrow (-n, -\alpha)$ and sketch in Figure 13 the curve of intermediate states (5.10) in (J, θ) -plane also indicating the essential n 's at which changes in stability type occur. Recall that for a given θ the relations (5.6) and (5.4) determine α and n .

The depicted trajectories have been obtained with the initial conditions $u = 0$, $v = 0$, $\theta = \pi - 0.01$, n is arbitrary, and α is one of the following: $\alpha = -(Cn - \sqrt{C^2n^2 - 4Amg\epsilon})/(2A) =: s_1(n)$, $\alpha = -(Cn + \sqrt{C^2n^2 - 4Amg\epsilon})/(2A) =: s_2(n)$, or $\alpha = -Cn/2A =: s_3(n)$. These choices were made to reduce to a minimum in the drawings the initial oscillations in the α -direction. We start near the equilibrium on the eigenvector of the

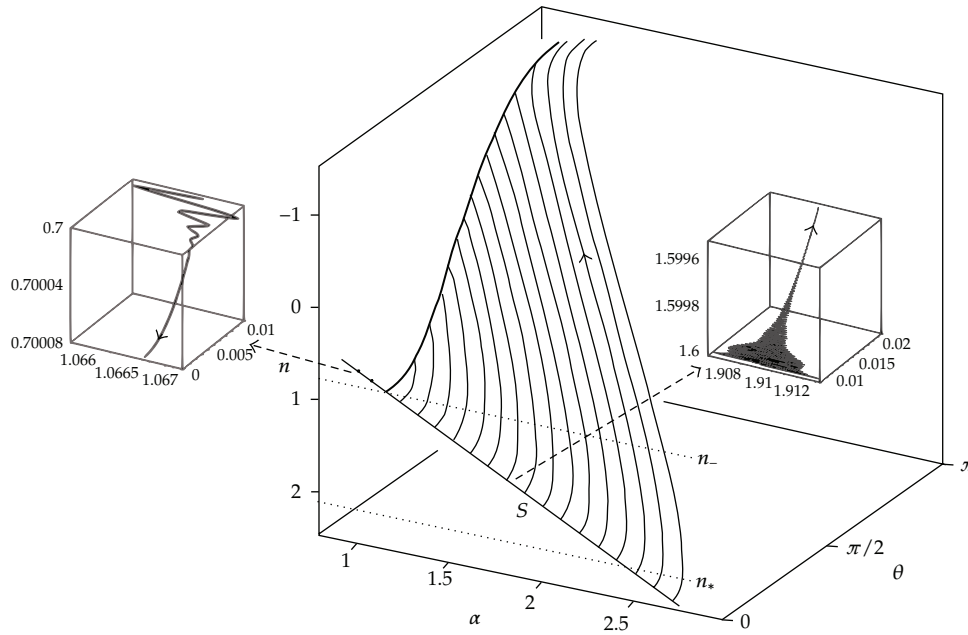


Figure 12: Trajectories of the system (3.15)-(3.16) projected onto the subspace of variables (α, θ, n) for an eccentric ball of Group IIb with friction $\mu = 0.04$. The bold-solid curve is that of intermediate states (5.4), (5.5), and (5.10); the line S in the (α, n) -plane represents the initial condition $\alpha = (1/2A)(Cn + \sqrt{C^2n^2 + 4Amg\epsilon})$. For $n > n_-$, fixed points on $\theta = 0$ are unstable. Trajectories are then attracted to a stable intermediate state (a point on the solid curve) for $n_- < n < n_*$ or to a point on the plane $\theta = \pi$ (i.e., flipping occurs) for $n > n_*$. The two insets are details at the starting position, one for the stable case and one for the unstable case. The parameters are chosen as $m = g = 1$, $\epsilon/R = 0.3$, and $A/C = 0.92$.

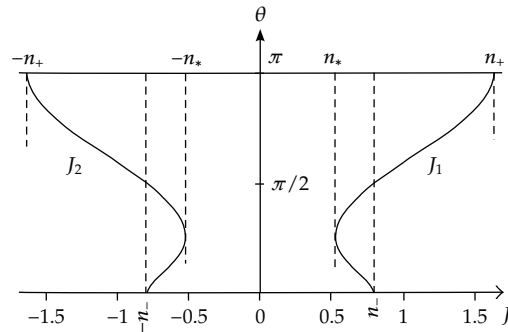


Figure 13: Curve of intermediate states (5.10) in (J, θ) -plane.

positive eigenvalue(s) so that the motion quickly evolves in the unstable direction away from the initial position. Trajectories originating near an unstable inverted position will either reach a stable intermediate state at $\theta > \theta_b$ when $n_b < |n| < n_+$ or fall in the noninverted vertical position when $|n| < n_b$. Here n_b is the value of the initial spin corresponding to the angle $\theta = \theta_b$ at which intermediate states change stability type. Points on $\theta = \pi$ with $|n| > n_+$ are stable and trajectories starting near the inverted state will be attracted to it.

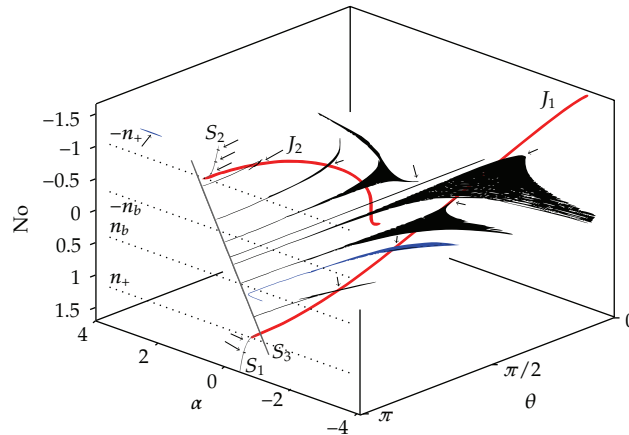


Figure 14: Trajectories of the system (3.15)-(3.16) projected onto the subspace of variables (α, θ, n) for an eccentric ball of Group IIa with friction $\mu = 0.04$. The bold curves are the intermediate states (5.10). The curves s_1 , s_2 , and s_3 in (α, n) -plane represent the curves on which the initial value of α is chosen. The starting angle is $\theta = \pi - 0.01$. The arrows indicate the final position. Points on the plane $\theta = \pi$ are stable if $|n| > n_+$, unstable otherwise. Trajectories are attracted to a noninverted position on the plane $\theta = 0$ for $|n| < n_b$, or they reach a point on the red curves otherwise. Two trajectories are added to illustrate the initial wild oscillations when α is not chosen on one of the s_i curves. We used $m = g = 1$, $\epsilon/R = 0.5$, $A/C = 0.55$, and $\mu = 0.04$.

7.2. 3D Animations

In this section we comment on the 3D animations illustrating the phenomena of “tipping” or “hanging on an intermediate state” for an eccentric sphere (<http://cage.ugent.be/~bm/tippetop/tippetop.html>). In the films, the eccentric sphere is drawn as a transparent ball with a top in it. We focus on eccentric spheres belonging to Groups IIb and IIa, see Figure 3 for the corresponding bifurcation diagrams. The films have been made using Maple to solve the ODE system and feeding the results to Povray, Imagemagick and ffmpeg. The films are in 5x slow motion for the sake of clarity, so 1 second takes 5 seconds in the animation, with 30 frames for every second. For the sake of clarity the evolution of the nutation angle θ is shown in each film.

The films for a top of Group IIb show a complete flip (See http://cage.ugent.be/~bm/tippetop/tippetop_IIb_flip.mpg), and the rising to a stable intermediate state (http://cage.ugent.be/~bm/tippetop/tippetop_IIb_IntSt.Comp.mpg) for a top of Group IIa the film shows how the top launched upside-down migrates to a stable intermediate state (http://cage.ugent.be/~bm/tippetop/tippetop_IIaComb.mpg).

In the first film one sees a complete flip (tippe top effect) of the sphere; the physical parameters used are $m = 6$ gram, $R = 1.5$ cm, $e/R = 0.5$, $A = 0.82$ mg/m², and $C = 0.7$ mg/m². The friction coefficient μ is 0.3. We show 90 seconds, which is presented as 7.5 minutes of the film.

The second film shows the motion towards a stable intermediate state from the unstable noninverted or unstable inverted position. The initial data is chosen so that the Jellett coincides with that of a stable intermediate state. It corresponds to 45 seconds of the tippe top movement. The physical parameters are here as in the first film except for the friction coefficient which is now $\mu = 0.1$. The initial conditions around $\theta = 0$ and $\theta = \pi$ are chosen

to correspond to a Jellett of approximately $0.84 \cdot 10^6$. The intermediate state is at $\theta = 134.5$ degrees.

The animations for a top out of Group IIa are meant to illustrate how, depending on the initial conditions, the top started at the inverted position ($\theta = \pi$) can fall either to an intermediate state or to the noninverted position ($\theta = 0$), see Figure 3. The physical parameters are $m = 6$ gram, $R = 1.5$ cm, eccentricity $e = 50\%$, $A = 0.385$ mg/(m²), and $C = 0.7$ mg/(m²). The friction coefficient μ is 0.08. In the left of the animation we see the behaviour in which the tippe top flips towards the noninverted state. However, oscillation of theta occurs. To the right, we see the movement for a slightly different initial state, with motion towards an intermediate state. Also here oscillation of theta occurs.

8. Further Remarks

Global Dynamics

Concerning Theorem 2.1 we wish to stress the importance of the local bifurcation diagrams for the global dynamics. Clearly, if we have a unique asymptotically stable ω -limit set it is clear that the basin of attraction for this set is equal to nearly the full measure set of the phase space defined by the complement to the stable manifolds of all coexisting (unstable) ω -limit sets.

It thus remains to analyze the situation when we have two coexisting asymptotically stable ω -limit sets. From the bifurcation analysis we know that in such case the coexisting stable ω -limit sets are the vertical states.

Theorem 8.1. *The ω -limit sets of the eccentric sphere on a flat surface with small friction are asymptotically stable relative equilibria (with respect to $SO(2) \times SO(2)$). The ω -limit set is a unique relative equilibrium, in which case the basin of attraction is the complement of the stable manifolds of the unstable relative equilibria (and hence dense, and of full measure, in the phase space). Otherwise, there are at most two stable relative equilibria (the vertical states) and the system is bistable. In this case, the union of the basins of attraction of the two vertical states is the complement of the stable manifold of the unstable relative equilibria, which is an intermediate state. This union is dense and of full measure in the phase space. The separatrix between the two basins of attraction (inside a level set of the Jellett invariant) consists of the stable manifold of an unstable intermediate state.*

Proof. Most of the above statement is a direct consequence of the existence of the energy as a Lyapunov function (through La Salle's principle). One readily verifies (from the local bifurcation analysis) that the stable manifold of the intermediate state coexisting with two asymptotically stable vertical states has codimension one (inside the level set of the Jellett invariant) and divides the phase space into two parts. \square

The regions of bistability (as a function of the Jellett invariant J) follow from the local bifurcation diagrams discussed in Theorem 5.1.

Remark 8.2. Note that the specific n 's where the changes in stability type of the steady states occur do not depend on μ . The viscous friction influences the time needed for an orbit to reach such a point. This fact was already clear in [13] and could be proved in advance also in our setup. The result remains true also for more general forms of friction laws proportional to V_Q such as those proposed in [4]. This suggests that the study of the asymptotic dynamics

of other (mechanical) problems, as for example the rattleback, might notably simplify by the introduction of viscous friction in the model.

Rolling Model

A “rolling” eccentric ball does not tip. In this section we give a simple argument showing that, if pure rolling is assumed, then the tippe top phenomenon cannot occur.

Solving the tippe top under the constraint of pure rolling (i.e., when the nonholonomic constraint $\mathbf{V}_Q = 0$ is satisfied) allows for complete reduction of the equations of motion to a second-order ode. See [3] for a discussion of this approach. In the pure rolling regime the system is not anymore dissipative and admits three conserved quantities: the energy, E , the Jellett J as before, and the Routhian, \mathcal{Routh} , given by [3]

$$\mathcal{Routh} = \left[\frac{1}{2}C + \frac{1}{2}mR^2\sin^2(\theta) + \frac{1}{2}m\frac{C}{A}(R\cos(\theta) - \epsilon)^2 \right] \omega_k^2. \quad (8.1)$$

“Tipping” in the rolling model would violate the conservation of \mathcal{Routh} . Indeed, from the Jellett invariant we know that the sign of ω_k has to change in a complete inversion since $\omega_k(\theta = \pi) = -((R - \epsilon)/(R + \epsilon))\omega_k(\theta = 0)$ and $R > \epsilon > 0$. But this is not allowed if $\mathcal{Routh} = \text{constant}$ has to hold.

The motion in the rolling model is governed by a functional relation of the type $\dot{\theta}^2 = f(\theta)$. Indeed, the conserved quantities give three relations for the components of the angular velocity ω_i, ω_j , and ω_k . In details, for a given θ , the Routhian (8.1) fixes ω_k , then the Jellett fixes ω_i , and finally the energy E fixes the tipping rate $\dot{\theta} = \omega_j$ (cf. (3.4)), yielding a functional relation of the type $\dot{\theta}^2 = f(\theta)$. Note further that the constraint $\mathbf{V}_Q = 0$ gives $U(\theta), V(\theta)$ from (3.9). In this approach, as mentioned in [3] one has to check whether a found solution is physically possible, that is, one has to take into account that rolling cannot be sustained if $|R_t| < \mu_s R_n$, where μ_s is the coefficient of static friction. In [3] it is remarked that only a few pure rolling precessional solutions satisfy this condition. The analysis, however, leaves open the possibility to have pure rolling periodic motions around the intermediate states as we discuss below.

Sliding versus Rolling

A debatable issue is whether transitions between sliding and rolling are possible during the motion of the top. As it was pointed out in [9], such transitions must also be considered when setting up a realistic model to describe the dynamics of the tippe top. To the different regimes there correspond different sets of equations. A switch between sliding and rolling occurs as the absolute contact velocity \mathbf{V}_Q vanishes. In the Coulomb-friction model, a switch from rolling to sliding occurs when the tangent reaction force required to maintain rolling exceeds $\mu_s R_n$. We refer to [4] for considerations and simulations on this topic and to [3] for a detailed analysis of the pure rolling model. We consider two test cases, the pendulum motion and the behaviour of the tippe top around a stable intermediate state.

- (i) The pendulum motion is easily observed by placing the tippe top on the ground, rotating it under an angle θ_s , and releasing it. We have $J = 0 = \mathcal{Routh}$ in this regime. Normally a pure rolling motion is observed. Only when θ_s is large, some slipping might be observed initially. Solved under the pure rolling constraint,

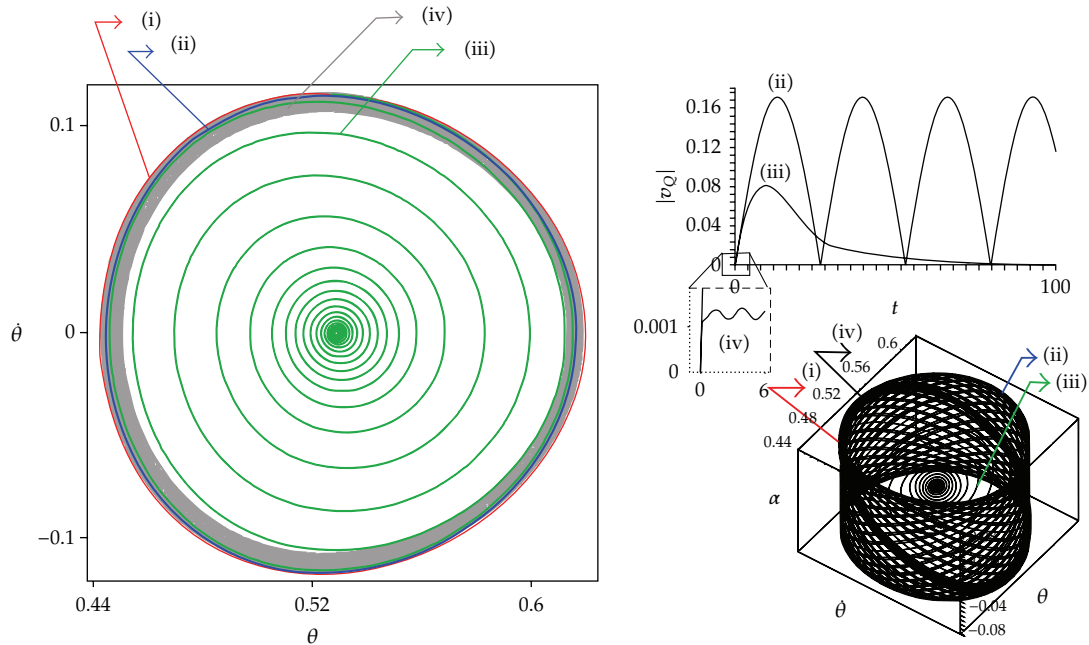


Figure 15: Periodic motion around intermediate state (IS) in $(\theta, \dot{\theta})$ frame, $m = 1 = g$, $\epsilon = 0.3R$, and $A = 0.92C$. Solution (i) is the pure rolling case for $J = 0.63$, $E = 1.1$, and $Routh = 0.33$, (ii) is the pure slipping case for $\mu = 0$ and (iii) is for $\mu = 0.1$, and (iv) for $\mu = 10$, the first 100 s. The data is chosen for a stable IS at $\theta_{IS} = \pi/6$, and the initial condition for (ii), (iii), and (iv) is a point on the solution curve of (i). For (i) a periodic motion is obtained, and for (ii) a quasiperiodic motion is observed as it is sketched in the $(\theta, \dot{\theta}, \alpha)$ frame. For $\mu > 0$ the trajectories spiral inwards towards the IS. For large friction, this motion is very slow (only the first 100 s is depicted). Also the speed at the contact point, $|v_Q|$, is given. In case (iii) this speed is large when far from the IS, and for (iv) this speed is very small corresponding to the very slow spiraling motion. Note that at $t = 0$, $v_Q = 0$ as it is expected.

the solution is pendulum-like. In contrast the sliding equation of motion (3.18), gives a qualitatively different solution. For $\mu = 0$, the solution is the pure sliding pendulum, where the center of mass remains fixed, but the tippe top makes a pure slipping periodic pendulum motion. (Recall that for $\mu = 0$ periodic solutions are possible, which was also clear from the Hopf bifurcation. However they all disappear when $\mu > 0$.) On activation of μ , we have that $\theta = 0$ is stable, and the slipping pendulum solution slowly degrades towards the stable point. In this case, the tippe top is best modeled with the pure rolling equations.

- (ii) Periodic motion around an intermediate state is characterized by the precession of the tippe top axle around the z -axis combined with a nutation $\theta(t)$ where $0 < \theta_m \leq \theta(t) \leq \theta_M < \pi$. In the pure rolling case periodic solutions can be obtained exactly. Using a point on this periodic solution as initial condition for (3.18) allows to investigate the persistence of this solution when friction is added, see Figure 15. For $\mu = 0$ a quasiperiodic motion is obtained around the pure rolling solution. Activating μ makes this motion unstable, and the solution goes towards the intermediate state, this behaviour is already dominant for $\mu = 0.1$ (note also the high $|v_Q|$ value). However, for ever larger μ the decay slows down, the solution remaining very long in the neighborhood of the pure rolling solution. The $|v_Q|$ value

in this case is very small, indicating that the condition for transition from slipping to rolling is satisfied.

Appendices

A. Proof of Theorem 5.1

For the interested reader, the following sections contain the calculations needed for a straightforward linear stability analysis of the steady states. These form the proof of Theorem 5.1.

A.1. Stability of the Vertical State $\theta = 0$

With the Taylor expansions in θ

$$Z_Q = -h(\theta) \approx -R + \epsilon - \epsilon \frac{\theta^2}{2} + O(\theta^3), \quad X_Q = h'(\theta) \approx \epsilon \left(\theta - \frac{\theta^3}{6} \right) + O(\theta^4), \quad (\text{A.1})$$

linearizing \mathbf{V}_Q in θ

$$V_{X,Q} \approx U - (R - \epsilon)\dot{\theta}, \quad V_{Y,Q} \approx V + nR\theta - (R - \epsilon)\dot{\phi}\theta, \quad V_{Z,Q} \approx 0 \quad (\text{A.2})$$

and noting that $R_n \approx mg$ and $n = \text{const}$, the linearization of the equations of motion (3.16) and (3.15) at $\theta = 0$ yields

$$\dot{U} - \dot{\phi}V = -\mu g(U - \dot{\theta}(R - \epsilon)), \quad (\text{A.3})$$

$$\dot{V} + \dot{\phi}U = -\mu g(V + Rn\theta - (R - \epsilon)\dot{\phi}\theta), \quad (\text{A.4})$$

$$A(\ddot{\phi}\theta + 2\dot{\phi}\dot{\theta}) - Cn\dot{\theta} = \mu mg(R - \epsilon)(V - (R - \epsilon)\dot{\phi}\theta + Rn\theta), \quad (\text{A.5})$$

$$A(\ddot{\theta} - \dot{\phi}^2\theta) + Cn\dot{\phi}\theta = -mg\epsilon\theta + \mu mg(R - \epsilon)(U - \dot{\theta}(R - \epsilon)). \quad (\text{A.6})$$

Introducing the complex coordinates

$$\xi = \theta e^{i\varphi}, \quad w = (U + iV)e^{i\varphi}, \quad (\text{A.7})$$

(A.3)–(A.6) can be reduced to two complex equations. The addition (A.3) + i (A.4) yields

$$\dot{w} = \mu g(-w + (R - \epsilon)\xi - iRn\xi), \quad (\text{A.8})$$

whereas i (A.5) + (A.6) leads to

$$A\ddot{\xi} - iCn\dot{\xi} = \mu mg \left((R - \epsilon)w - (R - \epsilon)^2\xi + iR(R - \epsilon)n\xi \right) - \epsilon mg\xi. \quad (\text{A.9})$$

These equations admit a solution of the form $(\xi, w) = (\xi, w)e^{\lambda t}$ when λ satisfies the determinant equation

$$D(\lambda, \mu) := -A\lambda^3 + \left(-\mu mg\epsilon^2 - \mu g^2 A + 2\mu mgR\epsilon + iCn - \mu mgR^2\right)\lambda^2 + \left(i\mu mgR^2 n - mg\epsilon + i\mu gCn - i\mu mgRn\epsilon\right)\lambda - \mu mg^2\epsilon = 0. \quad (\text{A.10})$$

When $\mu = 0$ the roots $\lambda(\mu)$ of (A.10) are

$$\lambda_1(0) = 0, \quad \lambda_{2,3}(0) = i\frac{Cn \pm S}{2A}, \quad (\text{A.11})$$

where we set

$$S^2 := C^2 n^2 + 4Amg\epsilon. \quad (\text{A.12})$$

In the absence of friction, that is, when $\mu = 0$, the vertical state $\theta = 0$ is marginally stable as $\lambda_{2,3}(0)$ are purely imaginary since $n^2 > -4Amg\epsilon/C^2$.

We now analyze the effect of small friction ($0 < \mu \ll 1$) by examining how the roots (A.11) are perturbed to first order in μ :

$$\lambda_1(\mu) = -\mu g, \quad \lambda_{2,3}(\mu) = \lambda_{2,3}(0) - \mu \left(\frac{mg(R-\epsilon)}{AS} [S(R-\epsilon) \mp ARn] \pm \frac{2m^2 g^2 \epsilon (R-\epsilon)^2}{S(Cn \pm S)} \right). \quad (\text{A.13})$$

As $\text{Re}(\lambda_1(\mu)) < 0$, the vertical state $\theta = 0$ is stable if $\text{Re}(\lambda_{2,3}(\mu)) < 0$. This is the case when

$$n^2 \left[\frac{A}{C} - \left(1 - \frac{\epsilon}{R}\right) \right] < \frac{mg\epsilon}{C} \left(1 - \frac{\epsilon}{R}\right)^2. \quad (\text{A.14})$$

It follows that, in Group I ($A/C < (1 - \epsilon/R)$), the vertical state $\theta = 0$ is always stable, while for Group II and Group III ($A/C > (1 - \epsilon/R)$) stability requires that $n_0 < n_-$.

It remains to be shown how $\text{Re}(\lambda_{2,3}(\mu)) < 0$ yields the relation (A.14). We focus on the inequality $\text{Re}(\lambda_2(\mu)) < 0$, the arguments are similar for $\text{Re}(\lambda_3(\mu))$. The inequality $\text{Re}(\lambda_2(\mu)) < 0$ yields

$$-\frac{1}{A} [S(R-\epsilon) - ARn] < -2mg\epsilon \frac{R-\epsilon}{Cn+S} \iff (Cn+S) \left(Rn - \frac{S}{A}(R-\epsilon) \right) < -2mg\epsilon(R-\epsilon). \quad (\text{A.15})$$

Using (A.12), this gives

$$\left(R - \frac{C}{A}(R-\epsilon) \right) (n^2 C + Sn) < 2mg\epsilon(R-\epsilon). \quad (\text{A.16})$$

Note that if $(R - (C/A)(R - \epsilon)) < 0$ the above condition is satisfied for all n . If on the other hand the inequality $(R - (C/A)(R - \epsilon)) > 0$ holds, then $(0 <)Sn < 2mg\epsilon(R - \epsilon)/(R - (C/A)(R - \epsilon)) - n^2C$; squaring both sides yields

$$n^2 < \frac{mg\epsilon}{A} \frac{R}{\mathcal{K}} (1 - \epsilon R)^2, \quad (\text{A.17})$$

where $\mathcal{K} := (R - (C/A)(R - \epsilon))$. Since we are in the case $\mathcal{K} > 0$, we can rewrite this last condition as (A.14).

Remark A.1. Ignoring translational effects, that is, throwing everything in the variable w away (cf. [5]), one is left with

$$\dot{w} = \mu(R - \epsilon)\dot{\xi} - i\mu R n \xi, \quad (\text{A.18})$$

$$A\dot{\xi} - iCn\xi = -\mu(R - \epsilon)^2\dot{\xi} - (\epsilon - i\mu R n)\xi, \quad (\text{A.19})$$

where we set for simplicity $m = 1$, $g = 1$. Equation (A.19) is of Maxwell-Bloch type [5] and allows us to recover the analysis carried out in [5]. An analogous result holds when linearizing around $\theta = \pi$.

A.2. Stability of the Vertical State $\theta = \pi$

The stability of the vertical state $\theta = \pi$ is studied in a similar way as in Section A.1. From the equation of motion (3.15)-(3.16), introducing complex coordinates

$$\xi = (\theta - \pi)e^{i\varphi}, \quad w = (U + iV)e^{i\varphi}, \quad (\text{A.20})$$

we obtain the coupled complex equations

$$\begin{aligned} \dot{w} &= -\mu g(w + (R + \epsilon)\dot{\xi} + iRn\xi), \\ A\dot{\xi} + iCn\xi &= \mu mg \left((R + \epsilon)w - (R + \epsilon)^2\dot{\xi} - iR(R + \epsilon)n\xi \right) + mg\epsilon\dot{\xi}. \end{aligned} \quad (\text{A.21})$$

The corresponding determinant equation for eigenvalue λ is given by

$$\begin{aligned} D(\lambda, \mu) &= -A\lambda^3 + \left(-2\mu mg\epsilon R - \mu gA - \mu mg\epsilon^2 - iCn - \mu mgR^2 \right) \lambda^2 \\ &\quad + \left(-i\mu mgR^2 n + mg\epsilon - i\mu gCn - i\mu mg\epsilon Rn \right) \lambda + \mu g^2 m\epsilon. \end{aligned} \quad (\text{A.22})$$

When $\mu = 0$, the roots $\lambda(\mu)$ of (A.22) are

$$\lambda_1(0) = 0, \quad \lambda_{2,3}(0) = -i \frac{Cn \mp S}{2A}, \quad \text{with } S^2 := C^2 n^2 - 4Amg\epsilon. \quad (\text{A.23})$$

Thus, at $\mu = 0$, the vertical state $\theta = \pi$ is at most marginally stable, when $\lambda_{2,3}(0)$ is purely imaginary, that is, when

$$|n| > 2 \frac{\sqrt{Amg\epsilon}}{C} =: n_*. \quad (\text{A.24})$$

This is of course also a necessary condition for stability if μ is small. Provided $S \neq 0$, corresponding to a resonance $\lambda_2(0) = \lambda_3(0)$ at $|n| = 2\sqrt{Amg\epsilon}/C$, the roots of (A.22) are perturbed at order μ to

$$\begin{aligned} \lambda_1(\mu) &= -\mu g, \\ \lambda_{2,3}(\mu) &= \lambda_2(0) + \mu \left(\frac{mg(R+\epsilon)}{AS} (-S(R+\epsilon) \mp AnR) \pm \frac{2m^2 g^2 e(R+e)^2}{S(Cn \mp S)} \right). \end{aligned} \quad (\text{A.25})$$

Thus, for stability we have to require $\text{Re}(\lambda_{2,3}(\mu)) < 0$, which yields

$$n^2 \left[\left(1 + \frac{\epsilon}{R}\right) - \frac{A}{C} \right] > \frac{mg\epsilon}{C} \left(1 + \frac{\epsilon}{R}\right)^2. \quad (\text{A.26})$$

Condition (A.26) is never satisfied for Group III, so $\theta = \pi$ is unstable. In the case of Groups I and II, when $A/C < (1 + \epsilon/R)$, the condition for stability is

$$n_\pi > \sqrt{\frac{mg\epsilon}{C[(1 + \epsilon/R) - A/C]}} \left(1 + \frac{\epsilon}{R}\right) =: n_+. \quad (\text{A.27})$$

Note that for tippe tops of Group I and II $n_+^2 \geq n_*^2$, with $n_* := 2\sqrt{Amg\epsilon}/C$. The equality $n_*^2 = n_+^2$ holds when $A/C = (1/2)(1 + \epsilon/R)$.

A.3. Stability of Intermediate States $0 < \theta < \pi$

In this section we consider intermediate asymptotic states, which exist if the condition (5.7) is satisfied. Such a state, if it exists, is of the form $v_0 = (0, 0, \bar{\alpha}, 0, \bar{\theta}, \bar{n})$, with $\bar{\alpha}, \bar{\theta}, \bar{n}$ constant and related by (5.4). In order to study the stability properties, we study the eigenvalues of the $SO(2)(\varphi)$ -reduced equations of motion, obtained from (3.18) by omitting the $\dot{\varphi}$ equation.

With J_0 denoting the corresponding Jacobian of this reduced equation, eigenvalues λ satisfy the determinant equation

$$D(\lambda, \mu) := \det(J_0 - \lambda I_6) = \lambda p_5(\lambda) = 0, \quad (\text{A.28})$$

where I is the (six-by-six) identity matrix and $p_5(\lambda)$ is a polynomial of degree 5 in λ . So, 0 is always a solution of (A.28).

Remark A.2. It is not possible to reduce the system to a ‘‘Maxwell-Bloch’’ form around an intermediate state as on the contrary was the case around the two vertical spin states.

When $\mu = 0$ the six roots of (A.28) are

$$\lambda_{1,2} = 0, \quad \lambda_{3,4} = \pm i\alpha_0, \quad \lambda_{5,6} = \pm i\alpha_0\sqrt{\mathcal{A}}, \quad (\text{A.29})$$

where

$$\mathcal{A} := \frac{A^2 + 2A\mathcal{B}\cos(\bar{\theta}) + \mathcal{B}^2}{A(m\epsilon^2\sin^2(\bar{\theta}) + A)} > 0, \quad \text{with } \mathcal{B} := (A - C)\cos(\bar{\theta}) + C\frac{\epsilon}{R}, \quad (\text{A.30})$$

and $\bar{\alpha}$ is given by (5.6). Note that $\mathcal{B} > 0$ from (5.7). All the eigenvalues λ_j , $j = 1, \dots, 6$ are on the imaginary axis, and the intermediate states at $\mu = 0$ are marginally stable.

Remark A.3. It is worth noting that for $\mu = 0$ the resonance $\lambda_{3,4} = \lambda_{5,6} = \pm i\bar{\alpha}$ occurs when $\mathcal{A} = 1$. Using the expressions for $\bar{\alpha}$ and \mathcal{A} given before, one checks that this equality is satisfied when the equation

$$\left[\left(\frac{A}{C} - 1 \right) \left(3\frac{A}{C} - 1 \right) + \frac{A}{C^2} m\epsilon^2 \right] \cos^2(\bar{\theta}) + 2\frac{\epsilon}{R} \left(2\frac{A}{C} - 1 \right) \cos(\bar{\theta}) + \frac{\epsilon^2}{R^2} - \frac{A}{C^2} m\epsilon^2 = 0 \quad (\text{A.31})$$

admits a real root between -1 and 1 . The resonance disappears when higher-order terms in μ are added.

When μ is small, $0 < \mu \ll 1$, we write the first-order perturbation of the roots as

$$\lambda_j(\mu) := \lambda_j(0) + \mu q_j, \quad j = 1, \dots, 6. \quad (\text{A.32})$$

From (A.28) it follows that

$$\begin{aligned} q_1 &= 0, & q_2 &= m^3 g^3 \epsilon^2 R^4 \sin^2(\bar{\theta}) g(\cos(\bar{\theta})) \mathfrak{D}\mathcal{E}, \\ q_3 &= q_4 = -mg, & q_5 &= q_6 = a_0(a_1 m + a_2), \quad \text{with } a_0 := \frac{m^3 g^3 \epsilon^2}{2A^2 R^2 \mathcal{B}^2 \mathcal{F}^2 \alpha_0^4 \mathcal{A}} > 0, \end{aligned} \quad (\text{A.33})$$

$\bar{\alpha}^2$ and λ_5 are as before and

$$g(\cos \bar{\theta}) := \left(\frac{A}{C} - 1 \right) + \frac{4 \left[(A/C - 1) \cos(\bar{\theta}) + \epsilon/R \right]^2}{(A/C) \sin^2(\bar{\theta}) + (\cos(\bar{\theta}) - \epsilon/R)^2}. \quad (\text{A.34})$$

The coefficients a_1 and a_2 are given by

$$\begin{aligned} a_1 &:= -\epsilon^2 \sin^2(\theta_0) \left[AR \left(R \cos^2(\theta_0) - 2\epsilon \cos(\theta_0) + R \right) - C \left(R \cos(\theta_0) - \epsilon \right)^2 \right]^2 < 0, \\ a_2 &:= AC^2 R^4 f \left(\frac{A}{C}; \frac{\epsilon}{R}, \cos(\theta_0) \right), \end{aligned} \quad (\text{A.35})$$

with

$$f\left(\frac{A}{C}; \frac{\epsilon}{R}, \cos(\theta_0)\right) := f_2 \frac{A^2}{C^2} + f_1 \frac{A}{C} + f_0, \quad (\text{A.36})$$

where

$$\begin{aligned} f_2 &:= -2 + 6 \frac{\epsilon}{R} \cos(\theta_0) - 5 \left(\frac{\epsilon^2}{R^2} + 1 \right) \cos^2(\theta_0) + 10 \cos^3(\theta_0) \frac{\epsilon}{R} - \left(1 + 3 \frac{\epsilon^2}{R^2} \right) \cos^4(\theta_0), \\ f_1 &:= -4 \frac{\epsilon}{R} \left(\frac{\epsilon^2}{R^2} + 2 \right) \cos(\theta_0) + 6 \left(1 + 3 \frac{\epsilon^2}{R^2} \right) \cos^2(\theta_0) - 4 \frac{\epsilon}{R} \left(4 + \frac{\epsilon^2}{R^2} \right) \cos^3(\theta_0) \\ &\quad + 2 \left(1 + 2 \frac{\epsilon^2}{R^2} \right) \cos^4(\theta_0) + 2 \frac{\epsilon^2}{R^2}, \\ f_0 &:= -\frac{\epsilon^2}{R^2} - \frac{\epsilon^4}{R^4} - 2 \frac{\epsilon}{R} \left(-1 - 3 \frac{\epsilon^2}{R^2} \right) \cos(\theta_0) + \left(-1 - \frac{\epsilon^4}{R^4} - 10 \frac{\epsilon^2}{R^2} \right) \cos^2(\theta_0) \\ &\quad - 2 \frac{\epsilon}{R} \left(-3 - \frac{\epsilon^2}{R^2} \right) \cos^3(\theta_0) - \left(\frac{\epsilon^2}{R^2} + 1 \right) \cos^4(\theta_0). \end{aligned} \quad (\text{A.37})$$

The coefficients $\mathfrak{D}, \mathfrak{E}$ are calculated with the help of Maple

$$\begin{aligned} \mathfrak{D} &:= \mathfrak{B}^2 - A \left(A - C + C \frac{\epsilon^2}{R^2} \right), \\ \mathfrak{E} &:= -\frac{(A - C)}{AB^2 \left[-m(R\epsilon\mathfrak{B} - \epsilon^2 C)^2 + R^2(C - A)^2(m\epsilon^2 + A) \right]}. \end{aligned} \quad (\text{A.38})$$

For tippe tops of Group II they have a fixed sign for θ_0 varying in $(0, \pi)$. Note that $q_{3,4} < 0$ and $q_{5,6} < 0$. The first inequality is obvious, and the second is less straightforward and is proved below. The friction is stabilizing at $O(\mu)$ when $q_2 < 0$.

The sign of q_2 depends on $g(\cos \bar{\theta})$ only, since the two terms $\mathfrak{D}, \mathfrak{E}$ are never zero for $0 < \bar{\theta} < \pi$. The zero of $g(\cos \bar{\theta})$ is the bifurcation point where the change in stability type happens. When $q_2 > 0$ the intermediate states are not anymore stable. For the sake of brevity we refer to [10] for the details on the behaviour of $g(\cos \theta)$, where the same crucial function is encountered in the stability analysis via the Routhian reduction. This analysis completes the proof of Theorem 5.1.

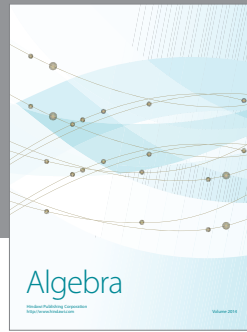
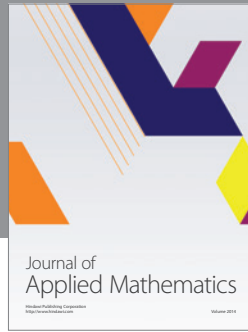
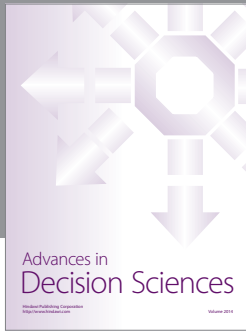
Proof of $q_5 < 0$. To prove that $q_5 < 0$ it is sufficient to prove that $a_2 \leq 0$, see (A.33), since $a_0 > 0$ and $a_1 < 0$. The sign(a_2) is determined by sign($f(A/C; \epsilon/R, \cos(\theta_0))$). Considering f as a square polynomial in A/C , $\tilde{f}(A/C)$, we have that the discriminant of $\tilde{f}(A/C) = 0$ is given by

$$\Delta_f := -\sin^2(\theta_0) \left(-1 + \frac{\epsilon}{R} \cos(\theta_0) \right)^2 \left[\left(\frac{\epsilon}{R} \cos(\theta_0) - 1 \right)^2 + \underbrace{1 - 2 \frac{\epsilon}{R} \cos(\theta_0) + \frac{\epsilon^2}{R^2}}_{>0} \right], \quad (\text{A.39})$$

which is negative for all θ_0 , ϵ/R . Hence, the sign of \tilde{f} remains fixed. It is easily verified that for $\theta_0 = 0, \pi$ or $\pi/2$, $\text{sign}(a_2)$ is always negative (e.g., $f(A/C; \epsilon/R, 1) = -2(\epsilon/R - 1)^2(\epsilon/R + 2(A/C) - 1)^2$), hence $a_2 \leq 0$ for all ϵ/R , A/C and θ_0 . We conclude that $q_5 \leq 0$. \square

References

- [1] J. Perry, *Spinning Tops and Gyroscopic Motions*, Dover, New York, NY, USA, 1957.
- [2] C. M. Cohen, "The tippe top revisited," *American Journal of Physics*, vol. 45, pp. 12–17, 1977.
- [3] C. G. Gray and B. G. Nickel, "Constants of the motion for nonslipping tippe tops and other tops with round pegs," *American Journal of Physics*, vol. 68, no. 9, pp. 821–828, 2000.
- [4] A. C. Or, "The dynamics of a Tippe top," *SIAM Journal on Applied Mathematics*, vol. 54, no. 3, pp. 597–609, 1994.
- [5] N. M. Bou-Rabee, J. E. Marsden, and L. A. Romero, "Tippe top inversion as a dissipation-induced instability," *SIAM Journal on Applied Dynamical Systems*, vol. 3, no. 3, pp. 352–377, 2004.
- [6] E. J. Routh, *Dynamics of a System of Rigid Bodies*, MacMillan, New York, NY, USA, 1905.
- [7] C. M. Braams, "On the influence of friction on the motion of a top," *Physica*, vol. 18, pp. 503–514, 1952.
- [8] J. H. Jellett, *A Treatise on the Theory of Friction*, MacMillan, London, UK, 1872.
- [9] T. R. Kane and D. Levinson, "A realistic solution of the symmetric top problem," *Journal of Applied Mechanics*, vol. 45, pp. 903–909, 1978.
- [10] M. C. Ciocci and B. Langerock, "Dynamics of the tippe top via Routhian reduction," *International Journal of Bifurcation and Chaos*, vol. 12, no. 6, pp. 602–614, 2007.
- [11] B. Y. M. Branicki, H. K. Moffatt, and Y. Shimomura, "Dynamics of an axisymmetric body spinning on a horizontal surface. III. Geometry of steady state structures for convex bodies," *Proceedings of the Royal Society of London. Series A*, vol. 462, no. 2066, pp. 371–390, 2006.
- [12] B. Y. M. Branicki and Y. Shimomura, "Dynamics of an axisymmetric body spinning on a horizontal surface. IV. Stability of steady spin states and the 'rising egg' phenomenon for convex axisymmetric bodies," *Proceedings of the Royal Society of London. Series A*, vol. 462, no. 2075, pp. 3253–3275, 2006.
- [13] S. Ebenfeld and F. Scheck, "A new analysis of the tippe top: asymptotic states and Liapunov stability," *Annals of Physics*, vol. 243, no. 2, pp. 195–217, 1995.
- [14] S. Rauch-Wojciechowski, M. Sköldstam, and T. Glad, "Mathematical analysis of the tippe top," *Regular & Chaotic Dynamics*, vol. 10, no. 4, pp. 333–362, 2005.
- [15] H. K. Moffatt, Y. Shimomura, and M. Branicki, "Dynamics of an axisymmetric body spinning on a horizontal surface. I. Stability and the gyroscopic approximation," *Proceedings of The Royal Society of London. Series A*, vol. 460, no. 2052, pp. 3643–3672, 2004.
- [16] R. Bastiaens, J. Detand, O. Rysman, and T. Deflo, "Efficient use of traditional-, rapid- and virtual prototyping in the industrial product development process," in *Proceedings of the 3rd International Conference on Advanced Research in Virtual and Rapid Prototyping (VRAP '09)*, Lleira, Portugal, 2009.
- [17] V. I. Arnol'd, *Dynamical Systems. Encyclopedia of Mathematical Sciences*, vol. 3, Springer, New York, NY, USA, 1988.
- [18] H. K. Moffatt and T. Tokieda, "Celt reversals: A prototype of chiral dynamics," *Proceedings of the Royal Society of Edinburgh Section A*, vol. 138, no. 2, pp. 361–368, 2008.
- [19] T. Tokieda, "Private communications," in *Proceedings of the Geometric Mechanics and its Applications (MASIE)*, Lausanne, Switzerland, July 2004.
- [20] C. Friedl, Der Stehoufkreisel, Zulassungsarbeit zum 1. Staatsexamen, Universität Augsburg, <http://www.physik.uniaugsburg.de/%18wobsta/tippetop/index.shtml.en>.
- [21] T. Ueda, K. Sasaki, and S. Watanabe, "Motion of the tippe top: gyroscopic balance condition and stability," *SIAM Journal on Applied Dynamical Systems*, vol. 4, no. 4, pp. 1159–1194, 2005.



Hindawi

Submit your manuscripts at
<http://www.hindawi.com>

